RSC Advances

REVIEW

View Article Online
View Journal | View Issue

Cite this: *RSC Adv.*, 2023, **13**, 29174

Recent development of piezoelectric biosensors for physiological signal detection and machine learning assisted cardiovascular disease diagnosis

Shunyao Huang,† Yujia Gao,† Yian Hu,† Fengyi Shen, Zhangsiyuan Jin and Yuljae Cho *

As cardiovascular disease stands as a global primary cause of mortality, there has been an urgent need for continuous and real-time heart monitoring to effectively identify irregular heart rhythms and to offer timely patient alerts. However, conventional cardiac monitoring systems encounter challenges due to inflexible interfaces and discomfort during prolonged monitoring. In this review article, we address these issues by emphasizing the recent development of the flexible, wearable, and comfortable piezoelectric passive sensor assisted by machine learning technology for diagnosis. This innovative device not only harmonizes with the dynamic mechanical properties of human skin but also facilitates continuous and real-time collection of physiological signals. Addressing identified challenges and constraints, this review provides insights into recent advances in piezoelectric cardiac sensors, from devices to circuit systems. Furthermore, this review delves into the integration of machine learning technologies, showcasing their pivotal role in facilitating continuous and real-time assessment of cardiac status. The synergistic combination of flexible piezoelectric sensor design and machine learning holds substantial potential in automating the detection of cardiac irregularities with minimal human intervention. This transformative approach has the power to revolutionize patient care paradigms.

Received 31st August 2023
Accepted 21st September 2023

DOI: 10.1039/d3ra05932d

rsc.li/rsc-advances

1. Introduction

Population ageing and consequent demographic change have brought significant challenges to the balance between economic growth and social care in virtually every country in the world. In particular, the pace of ageing in the Asia-Pacific region is unprecedented, with the rate of 14% in 2022 predicted to be 26% by 2050 of the older persons defined as those aged 60 years or over.[1] The elderly populations are particularly susceptible to cardiovascular diseases (CVDs) which are the leading cause of death in the world due to impaired quality of life, disability, and dependency.[2,3] By 2030, it is expected that the mortality rates due to CVDs will rise steadily from the current 17.9 million to 23.6 million people, posing serious challenges to public health.[4]

University of Michigan—Shanghai Jiao Tong University Joint Institute, Shanghai Jiao Tong University, Minhang District, Shanghai 200240, China. E-mail: yuljae.cho@sjtu.edu.cn

† These authors contributed equally to this work.

Shunyao Huang is a junior undergraduate student majoring in Electronic and Computer Engineering at UM-SJTU Joint Institute at Shanghai Jiao Tong University. Her research interests mainly include wearable sensing technology and machine learning.

Yujia Gao is a senior undergraduate student majoring in Electronic and Computer Engineering at UM-SJTU Joint Institute at Shanghai Jiao Tong University. She will pursue her graduate degree in the School of Information at the University of Michigan. Her research interest lies in flexible sensing technology.

As a large number of cardiovascular-associated mortalities can be prevented with early diagnosis and timely medical interventions, there has been a high demand for a real-time and long-term detection technology. However, current real-time monitoring devices such as Holter monitors with hard-wired and rigid interfaces are not suitable for the long-term detection because they are not light, compact, and comfortable to wear. Furthermore, the accuracy of measured data using the current monitoring devices is largely affected by daily body movement, and therefore it can be implemented only in a static state, limiting their practical applications. To solve the above issues, development of flexible/wearable and sensitive body pulse sensors converting physiological signals into electrical ones is of critical importance to perform real-time and continuous health monitoring to obtain long-term and accurate pulse waveforms. The most commonly and widely applied technique by now in the intensive care is the invasive arterial catheter, which can provide precise continuous body pulse and blood pressure monitoring. However, discomfort and potential risk of infection increase along with its accuracy of data during monitoring.

In this regard, non-invasive flexible/wearable health monitoring methods have received a great attention in recent decades.[5–10] As the non-invasive ones only contact human skin, the infection rate is greatly lowered, thus making them safe and widely applicable devices for daily base uses. A few types of flexible non-invasive biosensors have been developed and are categorized into an active and passive sensor. The active sensor needs an external power source to operate, and examples are photoplethysmography (PPG), capacitive, ionic liquid, and piezoresistive sensors.[11–17] In comparison, the passive sensor does not require an external power supply, meaning that they are self-powered, and the triboelectric and piezoelectric sensors are the typical examples of the passive sensor.[18,19] By eliminating the need for the external supply of power to operate the sensor, the passive sensor offers a great advantage over its counterpart active sensor for portable and wearable applications as they provide longer operation time.[16,20] Among the various passive sensors, the piezoelectric sensor has received significant attentions attributed to its higher response to strain than that of the triboelectric passive sensor, resulting from higher piezoelectric charge density than the triboelectric charge density at the same strain level. In addition, the piezoelectric sensor provides higher durability than that of triboelectric sensor. This is due to the existence of the air gap to be maintained in the triboelectric sensor, which increases the effective area affected by O_2 and H_2O molecules in the device.[16,21]

Along with the development of physiological signal sensing devices, recent advances in machine learning (ML) technology have significantly contributed to realization of CVD diagnosis. Various ML algorithms have been demonstrated to be effective to process body pulse data acquired from the cardiac sensors

Yian Hu is a junior undergraduate student majoring in Electronic and Computer Engineering at UM-SJTU Joint Institute at Shanghai Jiao Tong University. Her research interests include wearable devices and integrated circuits.

Zhangsiyuan Jin is a senior undergraduate student majoring in Electronic and Computer Engineering at UM-SJTU Joint Institute at Shanghai Jiao Tong University. She will pursue her master's degree at UM-SJTU. Her research interest includes wearable energy harvesting technology.

Fengyi Shen received his bachelor's degree from SJTU in 2023. He is currently enrolled in KTH Royal Institute of Technology in Stockholm for a master's degree in science. His research mainly covers energy harvesting, wearable electronics and MEMs.

Yuljae Cho is an associate professor at UM-SJTU Joint Institute at Shanghai Jiao Tong University. He received his PhD degree at the University of Oxford and was a research associate at the University of Cambridge. His research focuses on emerging energy materials and their applications to energy harvesting and optoelectronic devices.

and provide early warnings to patients. In addition, accuracy of CVD diagnosis has been improved through the implementation of real-time ML processing technique, leading to the innovation of the current medical practices in the future.[22] Flexible/wearable physiological sensors integrated with ML technology effectively process continuous and real-time data acquired and detect cardiac anomaly of body pulses, sending out alerts to healthcare professionals to provide prompt medical treatment. Not only for data processing, but ML technology also can be utilized to design and optimize flexible/wearable physiological sensors iteratively with respect to the desired medical cases to be treated, envisioning utilization of ML technology in advancing materials as well as device architecture levels in the future.[23]

Here, we present the recent progress in (1) flexible/wearable physiological sensors particularly based on the piezoelectric effect enabling self-powering of the sensors, (2) the management circuits for effective signal detection and processing, and (3) various ML algorithms to analyze data acquired by the sensors and ultimately diagnose CVDs for practical clinical validations. Since various reviews on flexible/wearable biosensors using mechanoelectric methods covering material and device engineering have been introduced previously,[24–26] we particularly direct our focus to the development of the whole medical system including sensors, circuits, and ML techniques. To start with, we introduce fundamentals of piezoelectricity including theories, mechanisms, and organic and inorganic materials. Then we turn our focus to the detection mechanism of health monitoring and the application of piezoelectric sensors to heart rate and blood pressure monitoring. Along with devices and circuits, we introduce various ML algorithms and their technologies for effective data processing and diagnosis of CVDs. Finally, an overview of current challenges to be addressed in both devices and ML technologies are discussed in prospective.

2. Piezoelectricity

2.1. Theory of piezoelectric effect

Among 32 crystalline classes in 230 space groups, 21 classes are categorized as non-centrosymmetric and 11 as centrosymmetric. Piezoelectricity is observed in 20 classes out of the 21 non-centrosymmetric classes.[27] Due to the non-centrosymmetric character, an electric dipole moment is created when a piezoelectric material is under external stimuli. The conversion of the mechanical input into the electrical output, or piezoelectricity, can be reversed, meaning that an electrical input will generate an internal mechanical strain, called the reverse (converse) piezoelectricity (Fig. 1a).

The piezoelectric and converse piezoelectric effects can be analyzed by the following eqn (1).[28]

$$\begin{bmatrix} \delta \\ D \end{bmatrix} = \begin{bmatrix} s^E & d^t \\ d & \varepsilon^T \end{bmatrix} \begin{bmatrix} \sigma \\ E \end{bmatrix} \quad (1)$$

In the eqn (1), δ and σ are strain and stress elements respectively; D and E are electric displacement and electric field components; s is the elastic compliance; ε is dielectric constant; and d is the piezoelectric coefficient. Superscript E and T mean that s and ε are measured under the constant electric field and constant stress, and t indicates transpose.

Piezoelectric materials show anisotropy in the piezoelectric coefficients. What affects this coefficient is the relative orientation between force and polarization direction. Therefore, the largest piezoelectric coefficients are obtained in ferroelectric materials through reorientation of electric dipoles.[29] The reorientation of electric dipoles can be achieved by applying an external electric field to the ferroelectric material, known as a poling process. Due to the poling, a net polarization is created by aligned electric dipoles, and the capacity to redirect the dipoles is required to create a net piezoelectric effect. In this regard, polycrystalline materials have advantages in generating the piezoelectric effect since the polycrystalline ferroelectric can have various orientations for the polarization vector. Thus, the possibility of one vector being aligned with the poling direction is greatly increased.[29]

The polar axis for a ferroelectric material is dependent on the poling direction, while for a non-ferroelectric one, the polar axis is defined by the crystal orientation.[30] The axis of a material is denoted as an axis 3 in Fig. 1b. Mechanical forces can be applied in two ways: (i) in parallel to the polar axis as the 3-direction or (ii) vertical to it, which is in the 1-direction in the figure. In the first case, the resulting configuration is named as 33-mode. Fig. 1b reveals that when the external stress or strain is applied

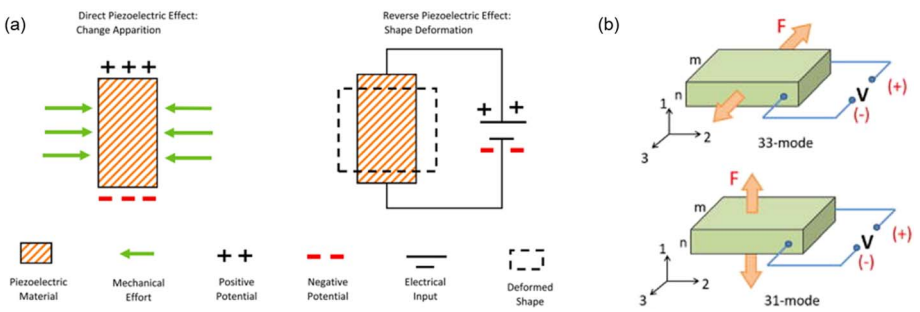

Fig. 1 Schematic illustration of (a) electromechanical conversion process by the piezoelectric effect (reproduced with permission from ref. 31 Copyright 2021 Elsevier), and (b) operation modes of the piezoelectric effect (reproduced with permission from ref. 30 Copyright 2018 AIP Publishing).

along the 3-direction, the voltage will be generated in the 3-direction as well. In the other case, the configuration is called 31-mode, whose working theory is illustrated in Fig. 1b. When the force is applied in the 1-direction, the resulting voltage will be created perpendicularly to the force, which is in the 3-direction. The piezoelectric coefficient (d_{31}) in the unit of C/N is used to quantify the piezoelectric performances of the materials, which is the ratio of the open circuit charge density to the applied stress.

In addition to the piezoelectric coefficient d, the electromechanical coupling factor k represents the ability of the material to do work *via* piezoelectricity as shown in eqn (2) where ε is the dielectric permittivity and s is the elastic compliance.[29–32]

$$k = \sqrt{\frac{\text{energy converted}}{\text{input energy}}}, \text{ or } k^2 = \frac{d^2}{\varepsilon \cdot s} \quad (2)$$

A prominent positive correlation between k and d can be observed for multiple materials. However, in contrast to the simple inference of eqn (2), the correlations between k and ε and s are also positive. This relevance can be illustrated when taking the form of d, ε, and s with respect to crystal chemistry parameters into consideration. This counterintuitive phenomenon can be explained by the relaxor-$PbTiO_3$-based single crystals which show the largest coupling factor k among all materials as well as extraordinarily large permittivity ε and compliance s.[29–32]

2.2. Piezoelectric response

It has been reported that there are two different mechanisms of the piezoelectric response: Intrinsic piezoelectric response; and extrinsic piezoelectric response. These two piezoelectric responses are attributed to polarization extension, polarization rotation, and motion of domain walls or phase boundaries.

First, the intrinsic piezoelectric response is induced by the polarization extension and polarization rotation. The polarization extension describes the change in the shape of a unit cell of the piezoelectric material when an electric field is applied parallel to spontaneous polarization (P_S), which is oriented along the positive c-axis. This electric field amplifies the magnitude of the polarization from its spontaneous value, and the interaction between strain and electric fields extends the unit cell as a result. Additionally, polarization extension contributes to the piezoelectric effects at the phase boundary between polar and nonpolar phases.[33,34]

On the other hand, the polarization rotation entails the reorientation of P_S from its remnant polarization, *i.e.* zero-field alignment, upon the application of the electric field. The ability to reorient P_S affects the property of piezoelectric materials. Specifically, the piezoelectric materials prone to the polarization rotation exhibit high permittivity perpendicular to P_S. In certain instances, the polarization direction may not be uniform within a specific domain.[35,36] This facilitates significant improvements in the piezoelectric response due to the electric field-induced polarization, even within what appears to be a single domain. The polarization extension and polarization rotation collectively define the observed piezoelectric response in a collection of appropriately oriented single-domain single crystals.

Second, the extrinsic response arises from the movement of mobile interfaces, such as domain walls or phase boundaries in response to the electric field applied.[37] When non-180° domain walls and phase boundaries traverse the material, they introduce alterations in the ferroelastic distortion. This results in changes in strain within the material.[38] Additionally, there can be smaller contribution, originating from the motion of 180° domain walls.[39,40] The extent of these extrinsic contributions to the overall piezoelectric response hinges on several factors, including the number of domain states dictated by the crystal structure, the Curie temperature (T_C), the microstructure of the sample, the domain arrangement, the chemistry of defects, and proximity to a morphotropic phase boundary.[41,42] Although the motion of domain walls can significantly augment the piezoelectric response, it is accompanied by hysteresis and the dissipation of energy within the piezoelectric material, resulting in degraded piezoelectric transduction efficiency.

2.3. Piezoelectric materials

Piezoelectric materials belong to a category of solid materials that are able to store electrical charges under mechanical pressure, making it possible to convert mechanical energy into electrical one and *vice versa*. In both inorganic and organic materials, the property of piezoelectricity has been discovered, and the characteristics of piezoelectricity differ with respect to the classification of the material.

2.3.1. Inorganic piezoelectric materials. The history of piezoelectricity in inorganic materials dates back to 1880 when Curie brothers found the piezoelectricity in quartz.[43] Several decades later in 1922, Rochelle salt (potassium sodium tartrate tetrahydrate) was found to be piezoelectricity as well, and various inorganic piezoelectric materials were discovered in subsequent years, such as barium titanium oxide ($BaTiO_3$, or BTO), aluminum nitride (AlN), zinc oxide (ZnO), and lead zirconate titanate (PZT). The mechanisms of inorganic piezoelectricity are illustrated in Fig. 2 by using examples of two typical materials, AlN and PZT. For these materials with an absence of symmetry in the crystal structure, the atomic structure of crystal changes under stress, leading to the creation of a non-zero crystal dipole moment. This non-zero dipole moment contributes to the permanent polarization of the piezoelectric materials even after the removal of an external electric field. The internal polarization has a linear relationship with the applied stress.

AlN is a tetrahedrally bonded semiconductor where the N atom is surrounded by four Al atoms in a tetrahedral interstice (Fig. 2a). The piezoelectric behavior in AlN arises from the spontaneous polarization along the c-axis. However, there exist two distinct dielectric domains in AlN, characterized by Al-polarity and N-polarity. In order to minimize the negative effect, Terai *et al.* proposed the pressure gradient sputtering (PGS) in fabrication of AlN films with high c-axis orientation and a single domain to improve the piezoelectric response,

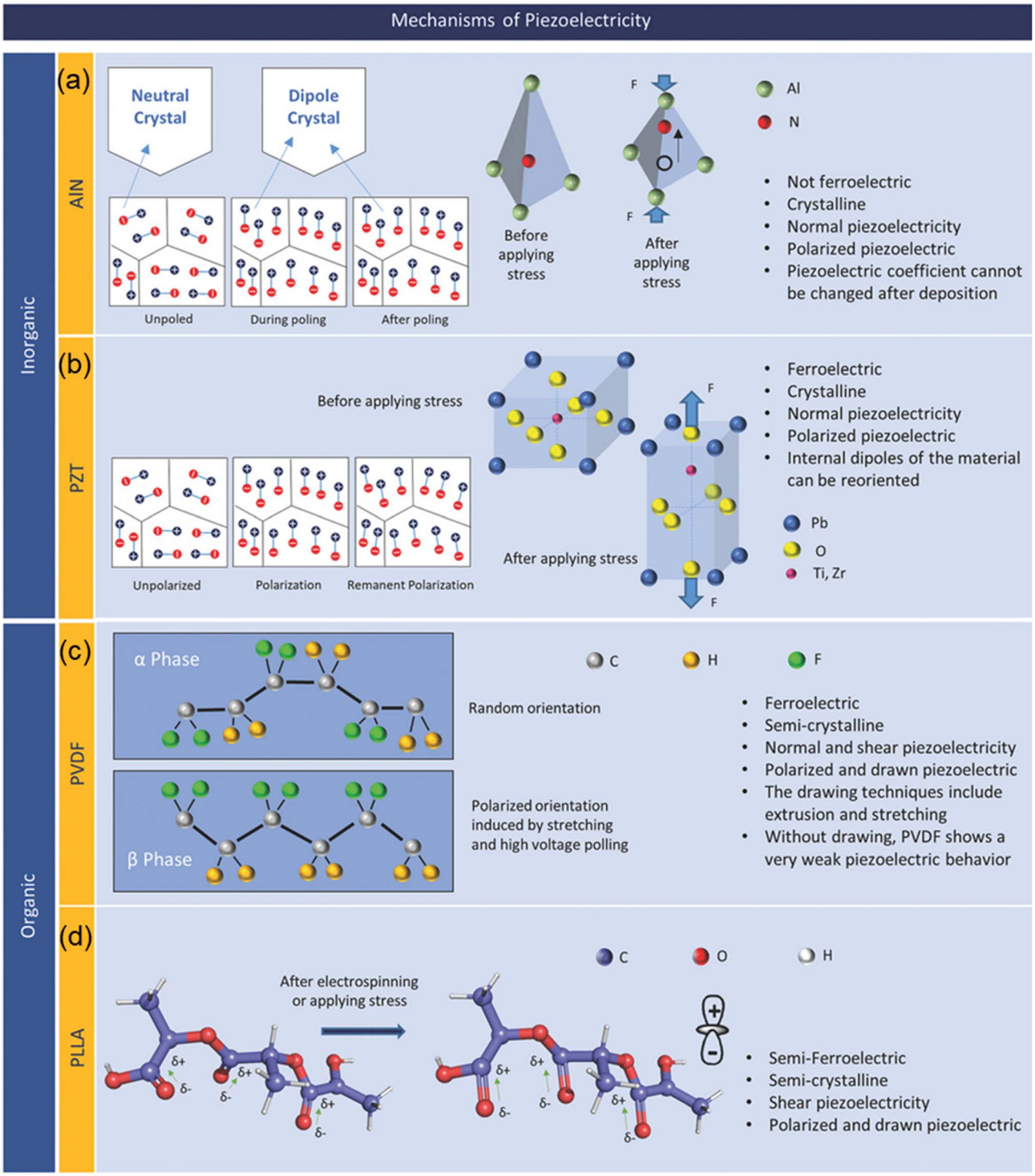

Fig. 2 Representative piezoelectric materials and their mechanisms: (a) AlN; (b) PZT; (c) PVDF; and (d) PLLA. Reproduced with permission from ref. 32 Copyright 2019 John Wiley and Sons.

contributing to a more precise measurement in biomedical signals detection.[44] AlN films have several advantages compared to other piezoelectric materials, such as better compatibility with standard CMOS processes, low-toxicity due to its lead-free nature, and high thermal stability. However, AlN has low piezoelectric coefficient d_{33} of 3–6 pC/N and d_{31} of −2 pC/N compared to its inorganic counterparts such as PZT.[45] For a crystalline AIN film, the crystal orientation of the film determines the piezoelectric coefficient and thus the coefficient cannot be changed after the formation of the film.

A perovskite BTO with the structure of ABO_3 was the first piezoelectric ceramic discovered in 1947 and has been widely

used for various ferroelectric and piezoelectric applications due to its high dielectric constant of 1500 – 6000, piezoelectric coefficient (d_{33} = 460 pC/N and d_{31} = 185 pC/N), and non-toxic character.[46,47] PZT is another example of the perovskite structure ferroelectric material and has a non-centrosymmetric crystal structure (Fig. 2b) with a non-zero net charge in its unit cell in an absence of external stimuli. As a ferroelectric material, in addition to its piezoelectric character, electric dipoles of PZT can be reoriented by an external electric field applied, resulting in a remnant polarization at zero bias condition.[48,49] PZT can be tailored to achieve soft (PZT-5H), semihard (PZT-4), and hard (PZT-8) PZT through various methods such as changing ratio of zirconia (Zr) content, doping acceptor (Mn) and donor (Nb) ions materials.[50–52] PZT, compared to its inorganic as well as organic counterparts, has a high piezoelectric coefficient of d_{33} = 300–700 pC/N. In spite of its high piezoelectric coefficient, inclusion of toxic substance Pb limits potential applications of PZT for biosensors. As an alternative to the PZT, a lead-free non-toxic $Na_xK_{1-x}NbO_3$ (NKN) piezoelectric ceramic was introduced. NKN has a favorable piezoelectric coefficient of d_{33} = 100–400 pC/N which can be further enhanced by doping the NKN ceramics.[53–55]

ZnO is an inorganic piezoelectric material with the wurtzite crystal structure where Zn^{2+} and O^{2-} are arranged in a tetrahedral shape and placed layer by layer along the *c*-axis.[56,57] The charge centers of cations and anions are aligned and that creates a coinciding effect. From the data of current researches, the piezoelectric effect for ZnO is relatively weak, compared to its inorganic counterparts, with the value of 6–13 pC/N for d_{33} and −5 pC/N for d_{31}.[58] Typical methods to improve the piezoelectric output behaviors include connecting several units in parallel or in series where the former one improves the output current while the latter one improves the output voltage. ZnO has a unique set of properties including excellent transparency, high electron mobility, and biocompatibility. However, high processing temperature of over 400 °C is required to fabricate ZnO-based devices which limits its application to some specific areas.[59]

2.3.2. Organic/polymer piezoelectric materials. Compared to inorganic piezoelectric materials, organic/polymer piezoelectric materials exhibit advantages in flexibility, biocompatibility, and environmental friendliness while they show low piezoelectric response.[60–67] For organic/polymer piezoelectric materials, the realignment of the molecular structure is a primary mechanism of the polarization under mechanical pressure.

Ferroelectricity and thus piezoelectricity in poly(vinylidene fluoride) (PVDF) was first reported in 1969 after the discovery of ferroelectric phenomenon.[68] PVDF has been widely used for a number of applications which require piezoelectric behaviors, such as energy harvesting, sensors, robotics, *etc.* due to its notable piezoelectric, ferroelectric, and pyroelectric properties together with its extraordinary biocompatibility and chemical resistance.[69–71] PVDF can be crystallized in four different phases, namely α-, β-, γ-, and δ-phase where only the β-phase with all-trans conformation shows ferroelectricity, and consequently pyroelectricity and piezoelectricity. Achieving a high concentration of the β-phase is desired to obtain PVDF with high responsivity to the applied stress/strain. The β-phase polymeric structure of PVDF is illustrated in Fig. 2. Piezoelectric coefficient of PVDF is reported to be in the range of d_{33} = 13–28 pC/N.[72]

By introducing molecular defects to PVDF monomer, intermolecular interactions can be altered and this modulates the physical properties of the PVDF polymer.[73] To date, defect modification has been widely implemented to produce various types of ferroelectric PVDF-based polymers, namely, copolymers and terpolymers with distinct behaviors in response to an applied electric potential. A typical example of a PVDF-based copolymer is P(VDF-TrFE), which can be synthesized through free radical polymerization of the two monomers, where TrFE is trifluoroethylene (TrFE) molecule.[74–76] Among PVDF-based polymers, P(VDF-TrFE) is the most widely used ferroelectric and piezoelectric polymer attributed to its enhanced piezoelectric coefficient d_{33} of 38 pC/N with 30 mol% of TrFE.[77]

Poly(L-lactic acid) (PLLA) polymer is a biodegradable polymer derived from plants, and it is often used in bioengineering. PLLA is a transparent and very flexible polymeric material, and thus is used for applications in mobile devices as an environmentally friendly, flexible, transparent, piezoelectric thin film.[78,79] Fig. 2 presents PLLA in the α-crystalline form which is thermodynamically stable conformation. In order to induce piezoelectricity, the chains must be thermally stretched to transform the α-crystalline form into the β-crystalline form, which represents a change from randomly oriented molecular chains to molecular chains being aligned along the stretched direction.[78,79] It is noted that elongated PLLA films have no

Table 1 Comparison of piezoelectric constants for various organic piezoelectric biomaterials[86–90]

Materials	Type	Electromechanical coupling factor k	Dielectric constant	Piezoelectric coefficient [pC/N]
AlN	Ceramic	0.06	∼8.63	d_{33} = 3–6; d_{31} = −2 (ref. 45)
BTO	Ceramic	0.34	∼7000	d_{33} = 460; d_{31} = 185 (ref. 47 and 58)
PZT	Ceramic	0.1–0.95	∼3000	d_{33} = 300–700 (ref. 50–52)
NKN	Ceramic	0.37	60–120	d_{33} = 100–400 (ref. 53–55)
ZnO	Crystal	—	∼10.4	d_{33} = 6–13; d_{31} = −5 (ref. 58)
PVDF	Polymer	14	∼10	d_{33} = −13–28; d_{31} = 23 (ref. 72)
P(VDF-TrFE)	Polymer	0.25	∼60	d_{33} = −38 (ref. 77)
Silk	Semi-crystalline	—	∼2.65	d_{14} = −1.5 (shear)[81,82]
Graphene	Single-layer	—	∼9.3	d_{33} = 1.4 [nm N^{-1}][85]

spontaneous polarization, unlike electrically poled PVDF as an example, but still have a large shear piezoelectric coefficient.[80] Although it has a complex higher ordered structure with intermingled crystalline and amorphous regions, it is possible to control the degree of crystallinity of PLLA through a thermal annealing process. Therefore, the piezoelectric constant of a PLLA film can be engineered and improved by increasing crystallinity and molecular orientation. This biodegradable and biocompatible film has many promising applications in the future of biosensors/actuators.

Silk has also shown the piezoelectricity, providing a great potential for wearable and bio applications. The origin of piezoelectricity in Silk is from the high degree of silk II, β-sheet crystallinity, and crystalline orientation. The shear piezoelectric coefficient of the silk film is reported to be $d_{14} = -1.5$ pC/N.[81,82]

Emerging 2D nanomaterials are another group of materials that are rapidly growing for biomedical applications.[83,84] Graphene has been found to have a piezoelectric effect recently and opened a great promise for piezoelectric biosensors due to the unique properties of the 2D nanomaterials such as high flexibility and stretchability.[85] Table 1 shows the summary of piezoelectric constant of inorganic and organic materials.

3. Piezoelectric sensor for health monitoring

3.1. Types of mechanoelectric sensor for health monitoring

The use of non-invasive devices for therapeutic monitoring of cardiovascular parameters not only enables the early diagnosis of CVD but also helps to improve the quality of life of patients. Non-invasive cardiovascular parameters are mainly measured by detecting pulse wave, electrocardiography (ECG), photoplethysmography (PPG), seismocardiography (SCG), ballistocardiography (BCG), *etc.* Among various sensors for health monitoring, mechanoelectric sensors have received great attention for detecting and measuring arterial pulse waves. The mechanoelectric sensors include resistive, capacitive, piezoelectric, and triboelectric sensors. Though different in mechanisms, the device configuration of the four sensors is generally in the similar structure composed of an active sensing component sandwiched between two electrodes (Fig. 3a–d).[91–94]

The principle of piezoresistive sensors is based on transducing the resistance change of a device into an electrical signal (Fig. 3a).[92] These sensors have undergone extensive research attention due to their simple device structures, convenient readout mechanisms, and the potential for achieving high energy density.[95] In addition, their adaptability to measure large strains over a wide range of pressures makes them reliable in various sensor applications. When external force (F) is applied to the sensors, contact resistance (R_C) is modulated with the relationship of $R_C \sim F^{-1/2}$, resulting in the changes in electrical signals. The piezoresistive sensors exhibit high sensitivity at low pressures, fast response speed, and large operating ranges.[96]

For capacitive sensors, the capacitance change is caused by the external stimuli (Fig. 3b) where the capacitance $C = \varepsilon_r\varepsilon_0 A/d$ with ε_r and ε_0 as constants standing for the relative permittivity of the material and vacuum permittivity, respectively. The capacitance change induced by the applied pressure is often used to control the frequency of an oscillator or vary the coupling of an alternating-current (AC) signal through a network. However, due to the relatively small change in the capacitance of parallel plates, the capacitive sensors typically exhibit low sensitivity.

Piezoelectricity, which arises from the presence of electric dipole moments in solids (Fig. 3c), is another commonly used transduction method for pressure sensors. Piezoelectric sensors are highly sensitive and exhibit rapid response times, making them valuable in detecting dynamic pressures such as mechanical vibrations. Attributed to its excellent mechanoelectric properties, the piezoelectric pressure sensors have attracted tremendous attention for various self-powered sensor applications.[97,98]

As for the triboelectric sensors (Fig. 3d), triboelectric charges are induced at the surface by the contact electrification and electrostatic induction when two different materials contact each other.[99,100] Using this effect, triboelectric sensors have been devised and widely utilized to achieve self-powered mechanical sensors in flexible/wearable forms. The triboelectric sensors generally show higher power output compared to other types of pressure sensors. However, unlike the piezoelectric effect, the triboelectric sensors require a constant change in forces, meaning that the sensors are suitable for dynamic force sensing but not static force detection. This is because the charges can

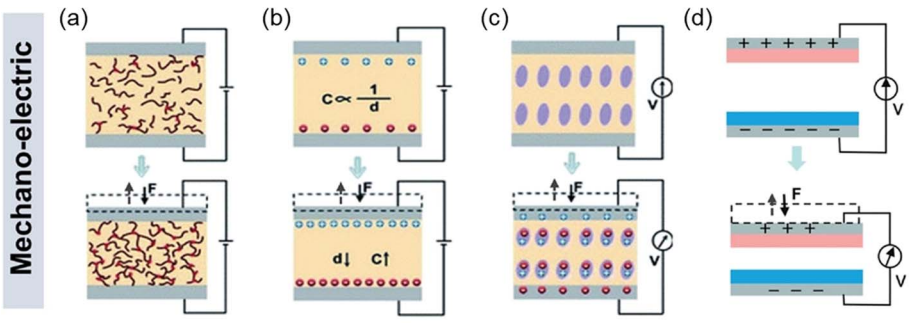

Fig. 3 Various mechanoelectric methods to detect body pulses: (a) piezoresistivity, (b) capacitance, (c) piezoelectricity, and (d) triboelectricity. Reproduced with permission from ref. 4 Copyright 2021 John Wiley and Sons.

only be transferred during the cycling of the contact and release of two materials with the opposite charges.

Among various mechanoelectric sensors, we particularly focus on the piezoelectric biosensors in this review as they offer several advantages over triboelectric, capacitive, and piezoresistive sensors when it comes to body pulse detection: (1) piezoelectric sensors are known for their high sensitivity, making them capable of detecting subtle changes in pressure or mechanical stimuli. This sensitivity is crucial for accurately capturing the dynamic nature of body pulses; (2) piezoelectric sensors exhibit rapid response times, enabling them to detect pulse signals in real time. This is particularly beneficial for monitoring physiological processes, where timely and precise measurements are essential; (3) in piezoelectric sensors, the mechanical pressure directly generates an electrical charge by the direct piezoelectric effect, simplifying the transduction process. This direct conversion allows for a more straightforward and efficient detection of body pulse signals; and (4) piezoelectric sensors can be self-powered, as the mechanical pressure applied to the sensor generates electrical energy. This feature eliminates the need for external power sources, making them more convenient for wearable and remote monitoring applications.

3.2. Working mechanism of piezoelectric sensor

The working mechanism of the piezoelectric biosensor is based on the polarization of electric dipoles in the piezoelectric materials. Fig. 4 illustrates the working mechanism of the piezoelectric sensor with two top and bottom electrodes as an example.[101] When there are no external stimuli applied to the sensor, a piezoelectric potential/field is electrically neutral and there is no generation of piezoelectric signal, *i.e.* electricity flow. When external stimuli, for example blood pressure is applied (Fig. 4a), piezoelectric materials will undergo deformations. This leads to a change in the crystal structure of the piezoelectric materials, and thus inducing polarization of electric dipoles. Due to the polarization, a piezoelectric potential/field is generated, and consequently electrical current is induced. When the external stimuli are released, deformation of crystal structure is restored and the piezoelectric potential/field will diminish and finally disappear; at this stage, a current with an opposite direction is induced. Similarly, when the piezoelectric biosensors experience bending by expansion of blood vessel as an example, the piezoelectric potential and consequently electric current are generated (Fig. 4b). The induced current density is proportional to the magnitude of pressure applied to the piezoelectric material/sensor and the piezoelectric coefficient d.

3.3. Physiological signals conversion

Physiological signals, *i.e.* body pulse waves, include two of the most important human body indicators which are blood pressure and heart rate. These physiological signals can be measured based on the local pressure and expansion of radial or carotid artery using the piezoelectric effect.

Heart rate (HR) can be derived from one of the multiple cardiac pulsating waves that demonstrate human heart's motions, such as pulse wave, ECG, PPG, SCG, BCG, *etc.* Among all these pulsating waves from the heart, pulse waves are the most frequently used signals in sensing techniques based on the piezoelectric effect. Pulse wave analysis (PWA) is an emerging technique for the assessment of arterial elasticity and has become an important technique for the early detection of arteriosclerosis. By wearing or patching the piezoelectric biosensors to the skin above one's artery, local vibration of the artery by cardiac motions can be detected, and this mechanical force will further be recorded and transformed into electric signals (Fig. 5a). This cardiovascular function index is based on the time-domain characteristics of the pulse waveform and the corresponding pathophysiological information.

Blood pressure (BP) is one of health indices which is directly related to cardiac motions. During the blood circulation process, arterial blood vessels are under periodic pressure by the cardiac motion. BP can be divided into two components that is systolic blood pressure (SBP) and diastolic blood pressure (DBP). Blood circulation throughout the artery leads to arterial pulses and consequent pressure fluctuations in a detectable way.[102] A typical pulse waveform is composed of the ascending and descending branch. The ascending branch results from a sudden expansion of the artery during ventricular contraction whereas the descending branch is caused by a ventricular

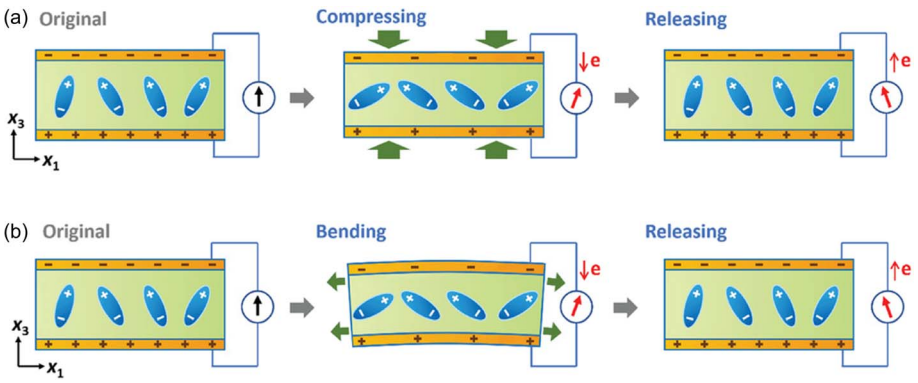

Fig. 4 Illustration of working mechanism of a piezoelectric sensor when (a) mechanical pressure or (b) strain is applied to the device. Reproduced with permission from ref. 101 Copyright 2022 John Wiley and Sons.

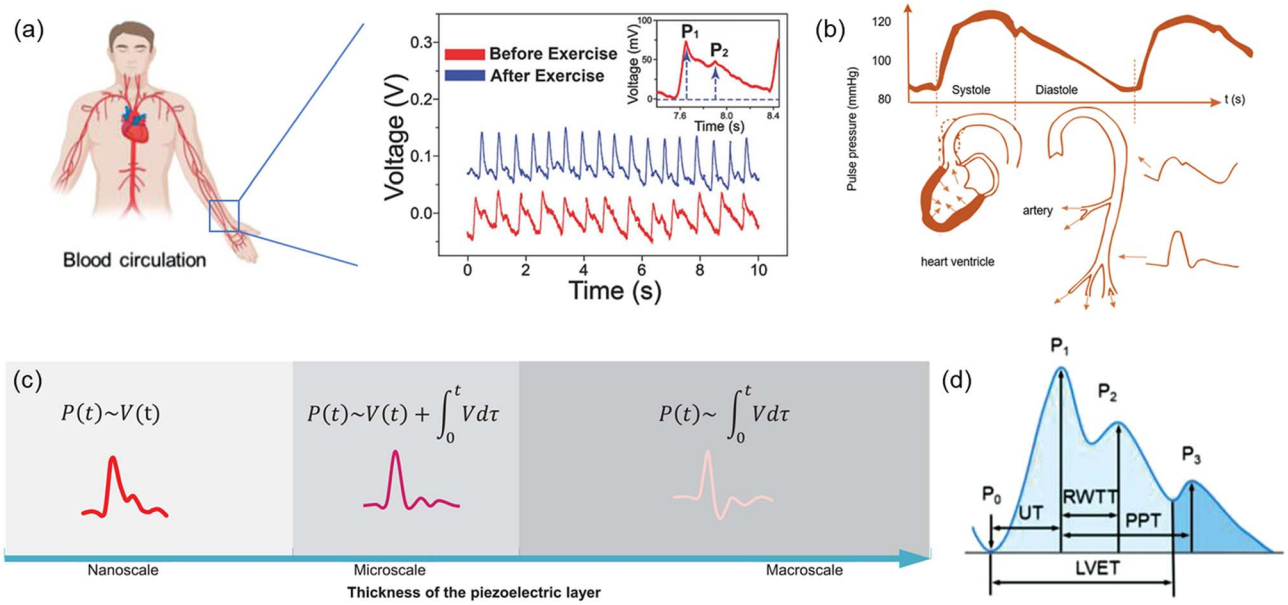

Fig. 5 (a) Artery and blood circulation in the human body. Reproduced with permission from ref. 106 and 118 Copyright 2017 and 2021 John Wiley and Sons. (b) The generation and propagation of body pulse waves, and illustration of factors affecting systolic and diastolic pulse waveforms. Reproduced with permission from ref. 104 Copyright 2022 John Wiley and Sons. (c) Typical possible arterial pulse waveforms by the piezoelectric effect. Reproduced with permission from ref. 105 Copyright 2022 John Wiley and Sons. (d) Typical pulse waveform of artery measured by the piezoelectric effect. Reproduced with permission from ref. 106 Copyright 2021 John Wiley and Sons.

diastole, as described in Fig. 5b.[103,104] Similar to heart rate, blood pressure is also based on the arterial pulses, and therefore, the typical waveform of blood pressure is similar to the pulse waves of heart rate. However, blood pressure may be affected mainly by two factors which are the transmission from arterial vessels to the skin surface and the body postures when measuring it. As a result, pulse waves attained from a piezoelectric biosensor have two correlations with blood pressure. In the first one, blood pressure correlates with the voltage transformed by the piezoelectric biosensor and its integration term in the period the pressure is applied on; the pulse waveform under this correlation may see a point as low as the starting point between the first and second systolic peak. In the second one, blood pressure correlates with only the integration form of the output voltage, and an inverse peak is followed by the first systolic peak in its waveform. Different correlations between piezoelectric response signals and the blood pressure can be obtained and transformed by changing the thickness of the piezoelectric layer in the sensor (Fig. 5c).[105]

3.4. Arterial pulse waveform and assessment of cardiovascular condition

Shapes of pulse waves measured in different human body parts may be slightly distinct, but most of them follow a typical form, which contains three peaks and one saddle point (Fig. 5d). One cardiac cycle begins from a trough related to the opening of the aortic valve (P_0), which is also the lowest point in the pulse wave. The pulse signal rises sharply to the first systolic peak (P_1) which is also the main waveform peak; at this point, arterial pressure reaches the maximum, making it the highest point in the whole pulsating process. Followed by the first peak but lower than it is the second systolic peak (P_2), which is also known as the reflection point or reflected wave peak. Then the pulse wave drops to the saddle points, or trough, which is composed of the rising and falling parts of the beat wave. Finally, pulse wave rises again and reaches the dicrotic peak (P_3); this third peak is lower than the second systolic peak, thus presenting the whole pulse wave in a descending trend. Among these four important points, the second systolic peak is the hardest one to detect. However, with its great clinical value, it has become the target for current researches for health monitoring and diagnosis.[105–108]

According to the pulse pressure waveform, the characteristic of the opening of the aortic valve (P_0), systolic peak (P_1), reflected wave peak (P_2), dicrotic notch, and diastolic peak (P_3) can be well selected as the feature points for the analysis of cardiovascular anomaly and disease. In clinical studies, values of UT, RWTT, PPT, LVET (Fig. 5d), PWV, SI, K, AI, HV, and HRV can be obtained from pulse pressure waveform.[109–111]

The systolic upstroke time, denoted as UT, is the time required for the upstroke of the pulse wave to reach the systolic peak. Although a higher UT value indicates lower elasticity of aorta, it should not be solely relied upon as the primary diagnostic index for arterial obstruction. Following the early systolic peak (P_1), the reflected wave generates the second wave known as the late systolic peak (P_2). The reflected wave transit time (RWTT) defines the return time and is calculated as the difference between the initial and reflected systolic wave peaks. PPT, on the other hand, represents the time difference between the early systolic peak (P_1) and the early diastolic peak (P_3) of the

pressure wave. Another relevant parameter, the left ventricular ejection time (LVET), measures the time difference between the opening and closing of the aortic valve, reflecting the cardiac function of systolic and diastolic capacities.

Pulse wave velocity (PWV) refers to the speed at which the pressure wave propagates through the vessel in the circulatory system, providing information on arterial compliance. It has been considered as a highly reliable prognostic parameter for cardiovascular morbidity and mortality in different groups of adult populations including renal disease, diabetes, and hypertension. It is calculated as eqn (3).[112,113]

$$\mathrm{PWV} = 0.8 \times \frac{2\Delta L}{\mathrm{RWTT}} \tag{3}$$

Similarly, the stiffness index (SI), eqn (4), is calculated by considering the velocity between the height of the tester (H) and the time delay of PPT.[114,115]

$$\mathrm{SI} = \frac{H}{\mathrm{PPT}} \tag{4}$$

Augmentation index (AI) is a metric used to assess systemic arterial stiffness and is derived from the upstroke aortic pressure waveform. As illustrated in eqn (5), AI is calculated as the difference between P_2 and P_1. The position of the reflection point in the aortic pressure pulse wave is primarily related to the stiffness of the blood vessel, which consists of the systolic upstroke wave (P_1), reflection wave (P_2), and dicrotic wave (P_3).

$$\mathrm{AI} = \frac{P_2}{P_1} \tag{5}$$

Stiffer blood vessels cause the reflection point to occur in an earlier time domain and at a higher-pressure domain. The form factor of the aortic pressure pulse wave is referred to as the characteristic K value and is associated with the mean pulse pressure, diastolic pressure (P_0), and systolic pressure (P_1). The K value can be defined as eqn (6) where T is the time duration of a complete pulse wave, P_0 is the diastolic pressure, P_1 is the diastolic pressure, and P_m is the mean pressure as illustrated in eqn (7).[116]

$$K = \frac{P_\mathrm{m} - P_0}{P_1 - P_0} \tag{6}$$

$$P_\mathrm{m} = \frac{1}{T}\int_0^T P(t)\mathrm{d}t \tag{7}$$

Heart rate representing the number of waveforms in a single minute is a widely used parameter for evaluating cardiovascular health. An independent parameter of heart rate variability (HRV) assessed by standard deviation of heart beat intervals (SDNN) illustrated as eqn (8) and (9) and Poincare plot has been adopted as a significant indicator to evaluate the risk of high cardiac death. The SDNN can be obtained using mathematical calculation of N beat-to-beat cardiac waveforms, T_1, T_2, …, T_N.

$$\mathrm{SDNN} = \sqrt{\frac{1}{N}\sum_{i=1}^{N}\left(T_i - \overline{T}\right)^2} \tag{8}$$

$$\overline{T} = \frac{1}{N}(T_1 + T_2 + \ldots + T_N) \tag{9}$$

The Poincaré plot is a scatter diagram of N cardiac cycles represented by a series of coordinates (T_1, T_2), (T_2, T_3), …, (T_{N-1}, T_N) with a comet-like elliptic shape. By fitting an elliptic curve to the scatter, the semi-minor axis and the semi-major axis can be obtained, marked as SD_1 and SD_2. These values have diagnostic significance for assessing the regulatory abilities of the parasympathetic and sympathetic nerves, respectively. Consequently, the value of $SD_{12} = SD_1/SD_2$ can be used to reflect the coordination of the sympathetic and parasympathetic nervous systems.[117]

4. Physiological signal detection using piezoelectric sensors

4.1. Heart rate

Currently, using piezoelectric sensors for heart rate monitoring is a popular topic in academia, and many research teams have devoted efforts to designing products that can fulfill this need. Though using different approaches, the main focus of study is to enable the sensor to perform continuous monitoring by wearing or patching it with a self-powered function so as to solve problems that current health sensors have such as inconvenience, bulkiness, unavailability in continuous health monitoring, *etc.* Therefore, piezoelectric biosensors have been made to improve wearability of the sensors through designing piezoelectric microfibers, to develop patchable piezoelectric biosensors that can be attached directly to human skins, to combine these two designing approaches together, or to develop a sensor managing circuit. Here, we introduce recent progresses in these aspects for continuous real-time heart rate monitoring.

One of the early works based on the piezoelectric effect for self-powered real-time arterial pulse monitoring was introduced in 2017 by Park *et al.* To resolve issues of low piezoelectric response of piezoelectric polymers, the authors employed inorganic piezoelectric PZT thin film for arterial pulse monitoring. The piezoelectric sensor showed a sensitivity of 0.018 kPa^{-1} with 60 ms of response time, and detected the radial and carotid artery pulses. Furthermore, a self-powered real-time pulse monitoring system was demonstrated by transmitting the pulse signal to a smartphone wirelessly, which opened up a great potential of the piezoelectric effect/sensor for biomedical applications. However, one concern is the inclusion of lead in PZT which is a toxic substance and not suitable for bio applications.[118]

Following the work from Park, in 2019, Chen *et al.* presented a flexible piezoelectric pulse sensor (PPS) with a simple sandwich structure based on a single-crystalline nitride thin film which is innoxious (Fig. 6a);[16] this solves the problem of using

the piezoelectric materials with toxic substances, such as lead. The introduced PPS exhibited high sensitivity and durability for flexible pulse sensor applications. The authors demonstrated that artery pulses from 10 different points were successfully measured by the PPS (Fig. 6b) with no signs of degradation. Furthermore, various physiological information was attained from the measured pulse waveforms, such as the pulse rate, AI, and PWV, through the pulse wave analysis. Similarly, Fu *et al.* take the attachability and bio-compatibility of sensors into consideration. The authors found the excellent properties of

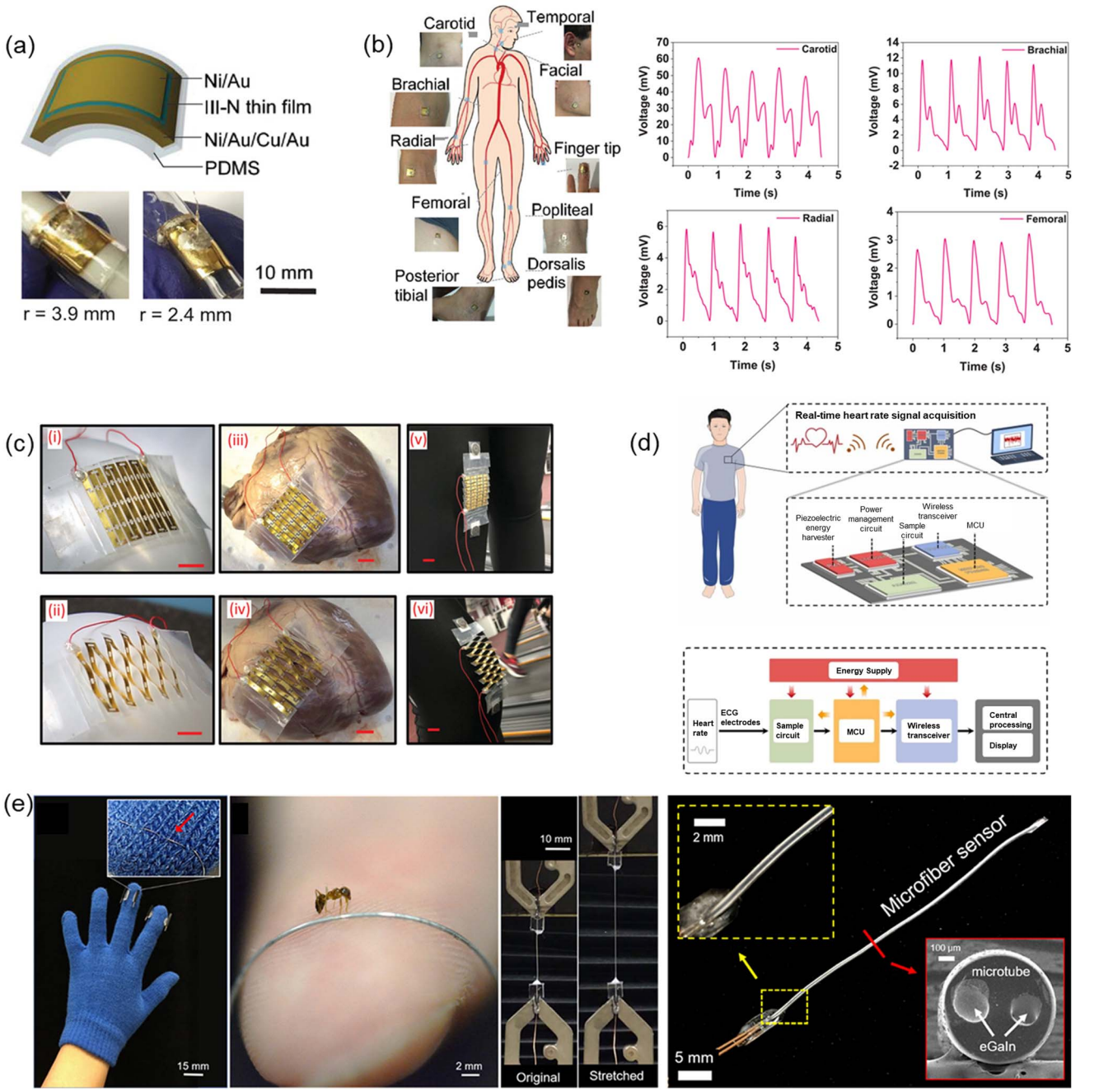

Fig. 6 (a) Structure and digital images of the III-N thin-film flexible PPS. (b) Body pulse waveforms measured by the III-N thin-film flexible PPS at various points on the human body. (a) and (b) Reproduced with permission from ref. 16 Copyright 2019 John Wiley and Sons. (c) Digital images of the stretchable sensor on various curved surfaces with a scale bar of 1 cm. Reproduced with permission from ref. 120 Copyright 2019 John Wiley and Sons. (d) Schematic illustration of the self-powered wireless body sensor system and the diagram of the system working flow. Reproduced with permission from ref. 122 Copyright 2022 Elsevier. (e) The digital picture of the piezoresistive microfiber-based glove; magnified image to compare the thickness of microfiber with an ant; demonstration of stretchability up to 120%; and an image of microfiber sensor and a cross section image of the sensor measured by SEM. Reproduced with permission from ref. 123 and 124 Copyright 2018 and 2019 American Chemical Society.

hydrogel, such as water-richness and great flexibility, and designed a self-powered piezoelectric polyacrylonitrile poly(-vinylidene fluoride) (PAN-PVDF) hydrogels. Hydrogel helps the sensor to have tighter contact with human skin, while PAN-PVDF is chosen as the sensing material due to its excellent piezoelectricity and plasticity.[119]

In vivo technology has also been introduced towards self-powered and wireless health monitoring based on the flexible and stretchable sensing system by Sun *et al.* in 2019.[120] The authors made an innovation through the introduction of kirigami technique (Fig. 6c), allowing the structural flexibility of the devices to robustly conform to various curved surfaces, such as heart and body joints. By introducing a novel intersegment electrode design, this integrated sensing system showcases excellent performances in both mechanical and electrical aspects. Also, the proposed system enables wireless data transmission to external devices by means of an embedded miniaturized wireless interface, which is not only of vital importance to implantable devices but can also achieve wireless and real-time health monitoring with no power needed for the sensor or the communication chip. These features have been evaluated through a range of practical assessments, including *in vitro*, *ex vivo*, and on body. The developed device is endowed with a promising future, for its novel features that can distinguish it from other sensing systems, as well as its contributions to the expansion of wireless monitoring of vital human signs and biomechanical health indicators.

As the sensing technique based on the piezoelectric effect is getting matured, an integration of measurement results with an analysis tool has gained attentions recently. In 2022, Samartkit *et al.* reported a non-invasive dynamic heart rate monitoring system based on a piezoelectric PZT sensor.[121] The authors developed an assistive software to perform continuous heart rate monitoring. It was demonstrated that the system could measure the heart rate with a mean absolute difference (MAD) and standard deviation of 1.78 and 1.98 beats per minute, respectively, with high accuracy. Similarly, a circuit design for better real-time heart rate signal collection has also been proposed by Wu *et al.* in 2022.[122] The authors realized real-time heart rate signal collection by integrating an energy supply module, electrocardiogram (ECG) electrodes, a sample circuit, a microcontroller unit (MCU) and a wireless transceiver (Fig. 6d). With the ECG electrodes and the sample circuit, heart rate signals could be sampled and would further be sent to a phone or computer through a wireless transceiver for processing and display. In the literature, Wu *et al.* discussed principles of building a nanogenerator based self-powered wireless sensor system and proposed a self-powered heart rate monitor with real-time operation. With the help of this system and the fast operation strategy of the device, satisfying performance of the heart-rate monitor was obtained with the reduced power consumption without affecting performance.

In addition to the piezoelectric sensors which are passive, piezoresistive and piezo-capacitive active sensors have also attracted tremendous research interests. For example, Yu *et al.* have reported a design of stretchable tubular elastomeric piezoresistive (STEP) microfiber. When pressure is applied, the resistance of the material will change, thus leading to the form of different shapes of heart rate pulse curves. It achieved piezoresistive by using the material of liquid eutectic Gallium Indium (eGaln) and storing it in a resilient microtubular structure. For the piezo-capacitive sensors, Yu *et al.* presented to implement a dual-lumen elastomeric microtube structure. This structure enabled the devices still functional to sense ambient pressure even when microfiber is cut in between due to its unique structure. This microfabric design also could be woven into other normal fabric products, such as the fingertips of gloves (Fig. 6e). With the gloves on, body pulses were successfully detected, and heart rate could be determined by calculating the frequency of detected pulses. Finally, it was demonstrated that the microfibers were washable and could even sense higher dimensional environmental information, such as position and directionality when weaving these microfibers into cross-stitched network.[123,124]

4.2. Blood pressure

Based on the theoretical studies in previous part, here, we introduce recent developments in biosensors for blood pressure measurement using the piezoelectric effect. Blood pressure monitoring can be divided into two strategies, invasive and non-invasive approaches. The invasive method can obtain more accurate blood pressure. However, due to concerns for infection, non-invasive measuring approaches are more often used in daily health inspections. Non-invasive blood pressure monitoring can be further classified into two types: cuff and cuffless approaches, where cuffless ones are more favored in daily lives and academic researches due to their portability and the ability to measure continuous real-time blood pressure.[125]

Using piezoelectric technology, biomechanical energy/signals can be efficiently transformed into electrical energy.[126–133] The principle of blood pressure measurement using the piezoelectric biosensors is based on the displacement of the tissue surface owing to the force of the pressure variation in artery. The arterial pulse piezoelectric dynamics technique involves three correlations for linking piezoelectric response to blood pressure: *via* integration, *via* transition correction, and *via* direct correlation. While this correlation was not initially well-defined in early studies, blood pressure monitoring using arterial pulse piezoelectric dynamics has gained substantial research attention. Here, we introduce recent developments in blood pressure measurement and analysis techniques based on the piezoelectric biosensors.

For biomedical applications, wearability is one of the prerequisites, and therefore devices in various forms have been researched. For example, Maity *et al.* demonstrated a PVDF nanofibers (NFs)-based piezoelectric sensor for self-powered human-health monitoring.[134] The authors introduced a piezo-organic e-skin sensor composed of the highly aligned PVDF NFs arrays, offering significant piezoelectric output performances for self-powered body pulse detection. The enhanced sensing capability results from combining well-aligned PVDF NFs arrays with PANI-coated PVDF NFs mat electrodes. As a result, the self-powered piezo-organic e-skin sensor holds

promise for various applications, covering routine health monitoring for diagnosis of CVDs. This innovation could mark a significant step forward in self-powered electronic skins and human–machine interfaces.

Very recently in 2023, Min *et al.* have reported a wearable piezoelectric blood pressure sensor and further demonstrated its clinical validation. Previously, the research group reported ultrathin epidermal piezoelectric sensors which successfully detected radial/carotid artery pulses, respiratory activities, and trachea movements by attaching the sensors directly on rugged skin.[135] However, challenges also have been identified to pursue continuous blood pressure monitoring because of the low signal and lack of a transfer function which can convert the signals into blood pressure values. In line with the previous work, the authors reported a new wearable piezoelectric blood pressure sensor (WPBPS) associated with an accurate blood pressure transfer function (Fig. 7a). The piezoelectric sensor is fabricated using PZT which has significant piezoelectric properties, leading to high sensitivity (0.062 kPa^{-1}) and fast response time (23 ms). Compared with existing FDA-approved medical instrument for continuous non-invasive arterial pressure (CNAP) monitoring, this CNAP can distinguish the shape of blood pulse waveforms more precisely. By using the transfer function of a linear regression model, the sensor signal was transformed into blood pressure values with high accuracy, validating its clinical values. This device makes it possible to monitor a person's body pressure continuously and precisely by integrating the device with the wristwatch (Fig. 7b and c).[135]

Similarly, Wang *et al.* reported a low-cost wearable piezoelectric-based system for non-invasive continuous beat-to-beat blood pressure measurement.[136] The device and measurement system developed was able to measure precise SBP and DBP without performing multiple calibrations and complex regression analysis. Beat-to-beat SBP and DBP monitoring was achieved by using the sum of initial blood pressure by an oscillometric method and pressure change by a piezoelectric sensor. Continuous pressure waveform was achieved by placing the piezoelectric sensor on the skin above the radio artery. Post-processing was then applied to locate significant feature points of SBP and DBP in order to determine the peak and valley of pressure pulse wave signal (PPW) (Fig. 7d). Voltage change and pressure change could be calculated accordingly. The results show that the measured mean absolute error (MAE) meets the criteria of the Association for the Advancement of Medical Instrumentation (AAMI) and British Hypertension Society (BHS), demonstrating its novel measurement strategy and effectiveness.[137,138]

In fact, the utilization of a piezoelectric effect for arterial pulse wave monitoring was first reported in 1941 and has attracted tremendous attention for several decades.[139–143]

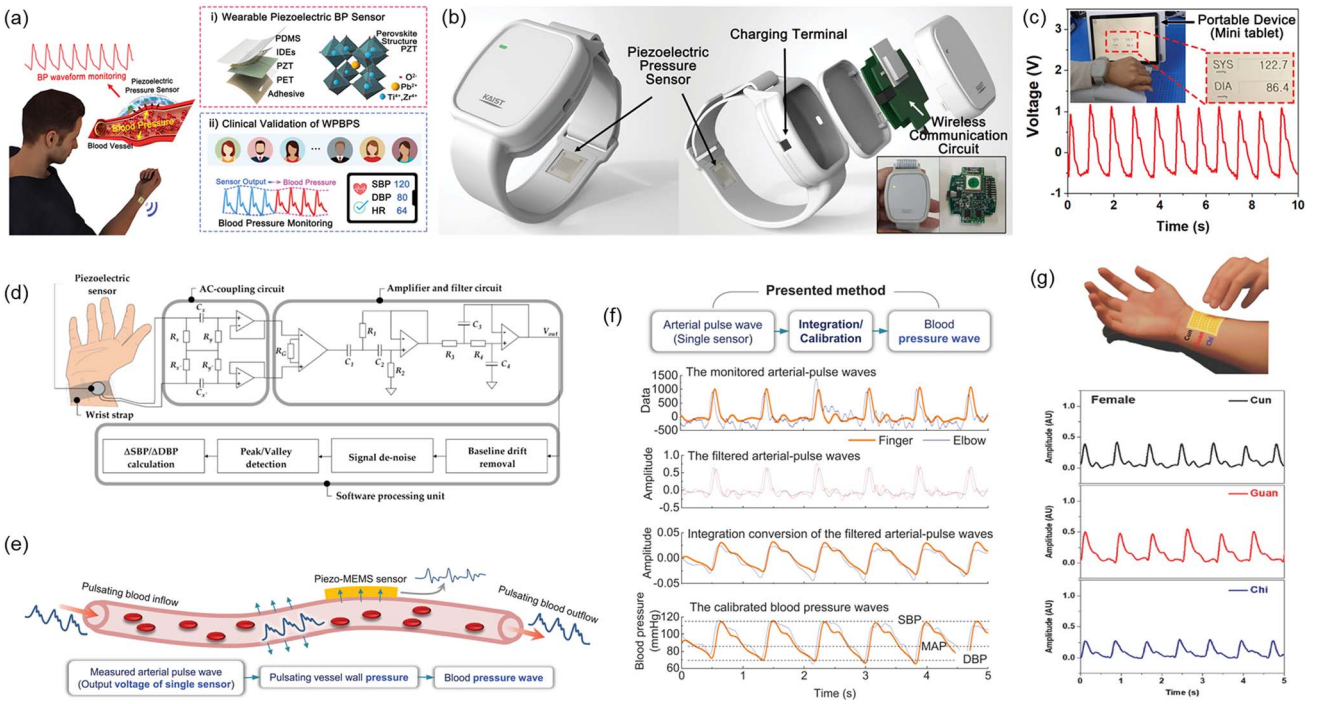

Fig. 7 (a) Schematic illustration of measurement of BP by a wearable piezoelectric sensor: (i) a structure of the piezoelectric BP sensor; (ii) a conceptual image of clinical validation. (b) Schematic illustration of the piezoelectric sensor-embedded wristwatch. (c) BP waveforms measured by the piezoelectric sensor and transmitted from the wristwatch by the wireless communication circuit where the inset shows beat-to-beat pulses and corresponding BP. (a–c) Reproduced with permission from ref. 135 Copyright 2023 John Wiley and Sons. (d) The piezoelectric sensor system composed of the piezoelectric sensor, front-end analog circuit, and software processing unit. Reproduced with permission from ref. 136 Copyright 2020 MDPI. (e) An illustration of arterial BP measurement using piezo-MEMS sensor. (f) Evaluation of BP waveforms through integration or calibration. (e) and (f) Reproduced with permission from ref. 105 Copyright 2022 John Wiley and Sons. (g) Illustration of the TCM pulse palpation acquisition scheme with the pulse sensing system and measured pulse waveforms at the Cun, Guan, and Chi positions. Reproduced with permission from ref. 146 Copyright 2018 John Wiley and Sons.

Nonetheless, the assessment of blood pressure using this method is inherently constrained due to issues such as time synchronization errors and distance inaccuracies among sensors positioned for monitoring by a minimum of two piezoelectric sensors. Unacceptably, the reported arterial pulse piezoelectric responses are largely inconsistent among studies, rendering the application of this technology for blood pressure monitoring contentious. To develop accurate wearable continuous blood pressure monitoring, it is therefore essential and urgent to elucidate the arterial-pulse piezoelectric response. Towards this goal, Yi *et al.* investigated the relationship between blood pressure waves and piezoelectric arterial pulse waves at nano-to macroscale thickness of the piezoelectric functional layer. The authors revealed that there are three correlations between blood pressure and piezoelectric response, which are integration, transition correction and direct correlation. The strategy, developed by the authors through filtering, integrating, and calibrating raw pulse data, can lead to continuous body pressure wave (Fig. 7e and f), thus making using only a single-sensor continuous blood pressure wave monitoring applicable. The single-piezoelectric sensor wireless monitoring system is also much more portable than traditional ones, suggesting its great promise as wearable continuous blood pressure monitoring for primary prevention and daily control of hypertension.[105]

Finally, physiological pulse wave sensing based on piezoelectric has also been explored recently. By definition, piezoelectrics refer to polymeric structures with electrically charged internal cavities. The piezoelectric effect, the same as the direct piezoelectric effect, converts mechanical energy to electrical one, allowing stress/strain sensing.[144,145] Chu *et al.* develop a flexible pulse wave sensing system based on a fluorinated ethylene propylene (FEP)/Ecoflex/FEP sandwich-structured piezoelectric with equivalent piezoelectric coefficient d_{33} up to 4100 pC/N. The high d_{33} value results from ample electrical dipoles maintained by FEP and the low Young's modulus for Ecoflex spacer. This device can measure the pulse at Cun, Guan and Chi pulse locations according to the traditional Chinese medicine practice (TCM), as marked in Fig. 7g. In real practice, the device is successfully used to diagnose arrhythmia among volunteers and detect blood pressure.[146]

5. Machine learning for health monitoring

With the aid of machine learning algorithms, identification of features of collected cardiovascular signals and implementing automatic classification of specific cardiac conditions have been progressed steadily in recent years.[147] The real-time data analysis and categorization enabled by machine learning assist to detect cardiovascular abnormalities in time, helping healthcare professionals diagnose CVDs and providing early medical interventions to potential patients (Fig. 8). Furthermore, machine learning marks a milestone in continuous health monitoring and an evolution in personalized health condition management.

5.1. Machine learning algorithms for CVD diagnosis

Machine learning is an analytical model that solves complex problems by executing a specific task without explicitly being programmed to do so.[148,149] During the machine learning process, the machine is required to learn a function injected from the input data (domain) to the labeled data (co-domain). Then the machine can utilize the learned function to make preferred choices when given any new datasets. Supervised learning, unsupervised learning, and reinforcement learning are three major types of machine learning. For supervised learning, training datasets are required to enable the machine to extract features of data and to derive a model. Then a trained machine can apply the acquired model and relationship to other new datasets for classification and prediction purposes. For unsupervised learning, there is no training for the machine to learn a model in advance. The machine classifies data and establishes structural information based on its own decision. For reinforcement learning, the machine is given a list of constraints and a clear goal. The machine accumulates data through trial-and-error methods and adjusts the strategies to maximize the reward in order to achieve the goal. To realize continuous real-time health monitoring for cardiovascular diseases, supervised learning is the preferred method to automatically classify specific cardiac conditions for collected cardiovascular signals.

For more complex cases, deep-learning-algorithms-based machine learning is applied to utilize automatic feature

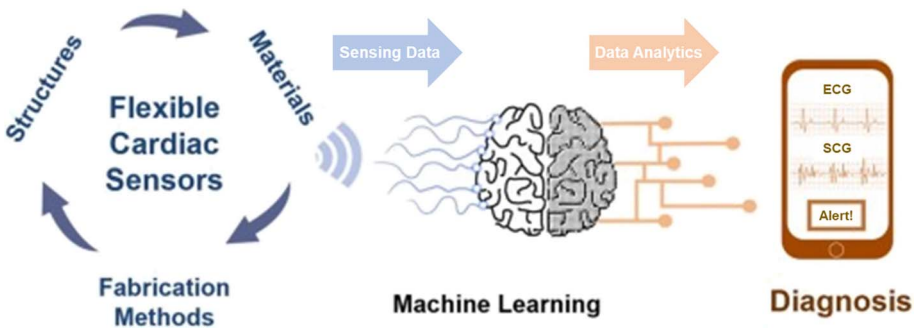

Fig. 8 Graphical illustration of the process of CVD diagnosis from sensing data using the sensors to data analysis by ML technique. Reproduced with permission from ref. 148 Copyright 2022 Elsevier.

extraction to implement classification (Fig. 9a).[150] Deep learning features multi-layer learning models with unstructured input data. The initial layers aim to extract low-level features whereas the last layers aim to extract high-level features for implementing classification and an additional level is used to improve the accuracy of classification. There are four major algorithms for categorizing cardiovascular sensing signals into specific cardiac conditions: convolutional neural network (CNN), hidden Markov model (HMM), Random Forest (RF), and binarized neural network (BNN).

For CNN (Fig. 9b), it consists of three main layers: convolution, pooling, and fully connected layer. The convolution layer accepts the input data and extracts the feature maps. Then the pooling layer down-samples the feature maps, which is always implemented by maximum pooling, to reduce network parameters and to minimize computation power as well as training time. In addition, common activation functions such as rectified linear unit (ReLU) and Leaky ReLU are utilized to apply complex mappings from input data to output data. Finally, the fully connected layer inherits the extracted features from the last convolution layer and matches them with different classes by calculating the probability for each specific class.

For HMM (Fig. 9c), it utilizes observation sequence and model parameters to derive the probability distribution of a hidden state sequence in order to implement categorization.[151] Each hidden state of the Markov model displays a specific probability of transitioning to next state (transitional probability) and a probability corresponding to the observed variables (emission probability). With probability values calculated, the HMM algorithm chooses the optimal path and links the hidden sequence corresponding to the observed sequence to execute classification.

For RF algorithm (Fig. 9d), it consists of multiple random decision trees.[152] Each decision tree chooses a random subset of training data as the training set and randomly chooses a subset of all features as the classification standards at split nodes. After continuously traversing all possible split points of the feature subset of this tree, each decision tree chooses the best split features as the optimal classification standard. Then the forest model lets each decision tree vote the classification standard of all decision trees to decide the final choice.

For BNN, it uses +1 and −1 to denote weights and activation functions. This algorithm has features of a significantly reduced memory size and computational power by utilizing bit-wise operations.

All these four algorithms have their own advantages while implementing classification. CNN features relatively accurate classification outcomes with relatively low computational power. HMM allows for no training datasets and predicts unknown classification from observed variables directly. RF features accuracy and stability of the model as well as prevents over-fitting effectively. BNN stands for high efficiency with reduced memory size and computational power. All four algorithms have a great potential in cardiovascular sensing field.

5.2. Implementation of ML for CVD diagnosis

The biosensor system has been widely applied to achieve the real-time and continuous health monitoring. Machine learning is then combined to do classification and recognition of

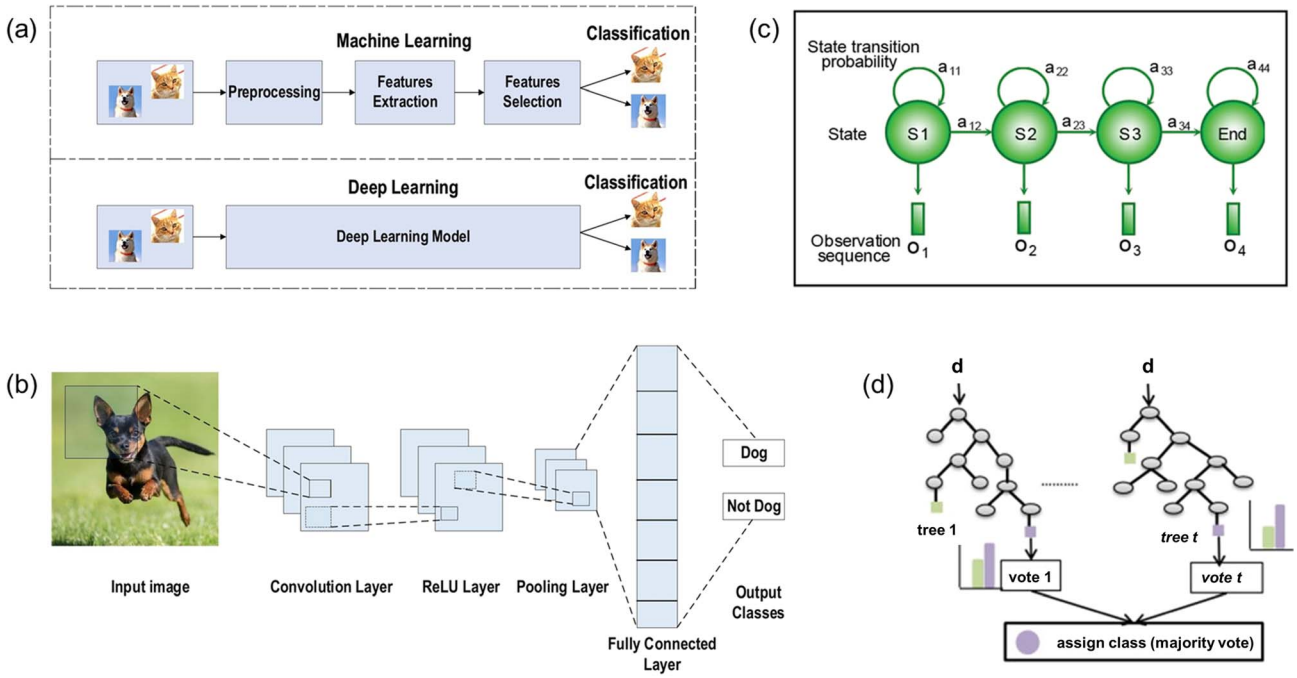

Fig. 9 (a) Illustration of difference between the machine learning and deep learning processes. Illustration of structures of various ML algorithms: (b) CNN model; (c) HMM model; and (d) random forest model. (a) and (b) Reproduced with permission from ref. 150 copyright 2021 Springer Nature. (c) Reproduced with permission from ref. 151 Copyright 2019 John Wiley and Sons. (d) Reproduced with permission from ref. 152 Copyright 2016 Elsevier.

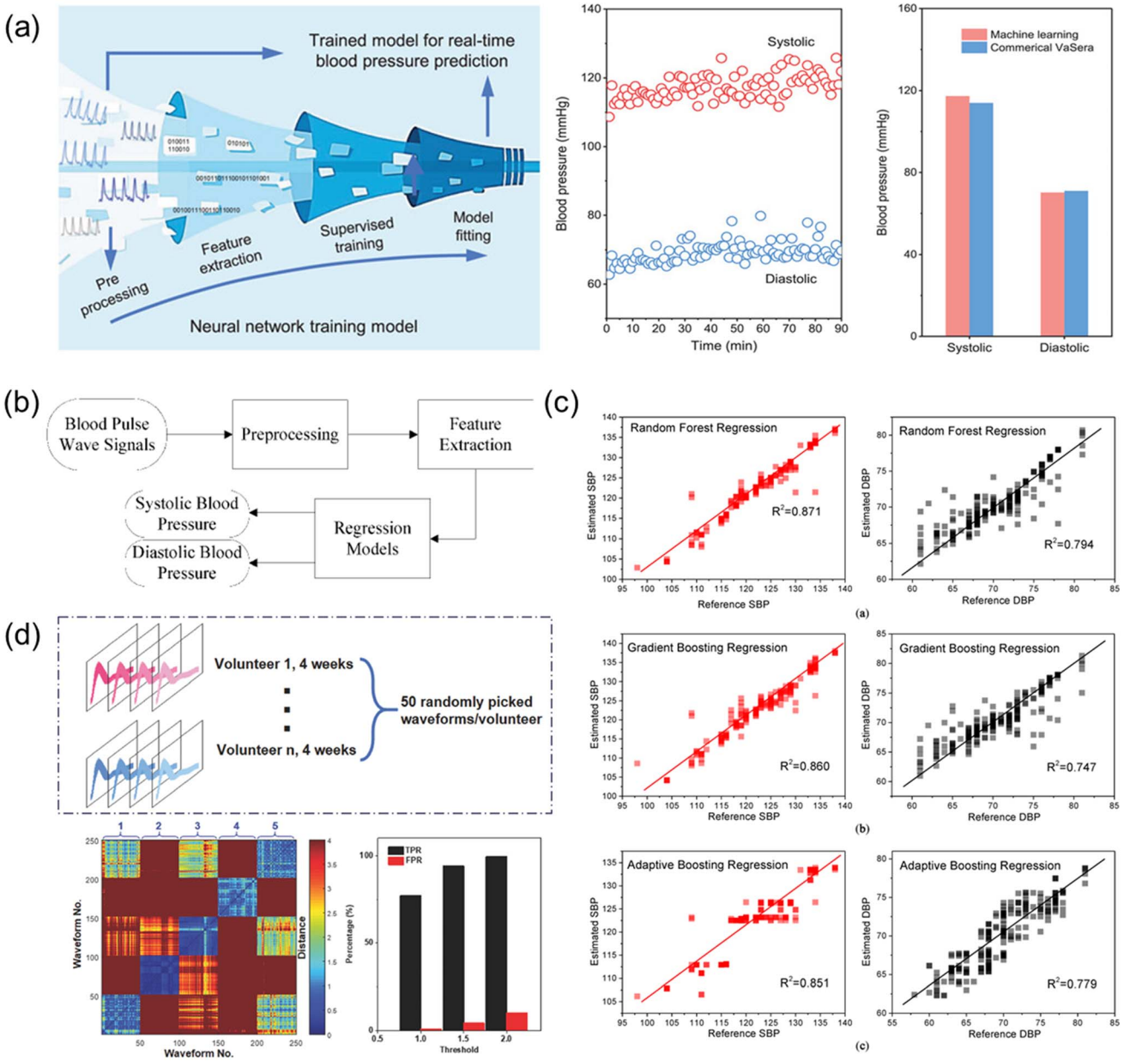

Fig. 10 (a) Illustration of ML technique to estimate blood pressure, and comparison of the blood pressure attained by the ML technique and the commercial device. Reproduced with permission from ref. 106 Copyright 2021 John Wiley and Sons. (b) Block diagram illustrating ML technique to estimate the blood pressure. (c) Results of the estimated SBP and DBP using different regression algorithms, namely, Random Forest Regression, Gradient Boosting Regression, and Adaptive Boosting Regression. (b) and (c) Reproduced with permission from ref. 153 Copyright 2019 MDPI. (d) ML technique to differentiate pulse wave signals attained by the wearable piezoelectric sensors. Reproduced with permission from ref. 146 Copyright 2018 John Wiley and Sons.

abnormal data collected by the sensors. Classification of different patterns helps link different abnormal signals to corresponding symptoms, which enables early diagnosis of CVDs. Detailed examples of ML technologies for health monitoring and diagnosis are illustrated in Fig. 10.

First, a feedforward neural network features a simple structure and a one-way propagation as illustrated in Fig. 10a. This ML method can accurately implement any finite training sample set, ensuring a high accuracy in classification and prediction based on the model learned. A supervised feedforward neural network can be utilized to simulate and predict both SBP and DBP of the arterial pulse waves collected by the biosensor as reported by Fang *et al.* in 2021.[106] By using the trained neural network model, the authors attained SBP and DBP of 117.3 and 70.2 mmHg with standard deviations of 3.06 and 3.50, respectively (Fig. 10a), demonstrating the high reliability of ML for monitoring blood pressure.

Second, regression is a statistical method to analyze the relation between two data sets and establish a model to link the factors to the corresponding outcomes. The ML regression

methods include RF regression, GBTD regression, and Adaboost regression. RF regression trains decision trees on randomly selected samples, using various features for partitioning and aggregating predictions. GBTD regression reduces losses iteratively, compensating for model limitations. Adaboost regression is an iterative process using all samples, assigning weights and focusing on difficult classifications. These regression techniques classify pulse wave signals to diagnose CVD symptoms, allowing early diagnosis outside hospitals, transforming monitoring systems comprehensively. Recently, Yang *et al.* demonstrated the estimations of SBP and DBP using various regression models (Fig. 10b).[153] Fig. 10c illustrates the correlation analysis between the reference blood pressures measured by using a cuff sphygmomanometer and the estimated blood pressures based on various regression models. The estimated SBP and DBP by the various regression models were found to be the most accurate with the RF regression model in the study.

Third, DTW (dynamic time warping) algorithm is widely applied to determine the degree of the similarity of two different time series. This algorithm requires a classified data set as a template, and for every point in the newly input data set the algorithm will calculate the distance between the point and every other point of the template set (Fig. 10d).[146] For each pair of pulse waves, a DTW distance is calculated to reflect the similarity and the minimum DTW distance indicates the highest similarity, further affecting the decision of classification. Fig. 10d shows the analysis results from five volunteers participated in the study. The red color region indicates high dissimilarity between two pulse waves and the blue color region means high similarity. The five blue squares along the diagonal axis illustrate that the pulse waves acquired for continuous 4 weeks are stable with high similarity for the same volunteer. The other squares show the variances and dissimilarities of pulse waves from different volunteers. By setting the threshold at different distances, the identification process for the true positive rate (TPR) and false positive rate (FPR) can be adjusted for a specific purpose, as indicated in Fig. 10d. The differentiation and classification of the pulse wave demonstration also proves the excellent stability and precision of the pulse sensing system for possible long-term health data collection from different users.

6. Perspectives

Recent achievements and breakthroughs in wearable piezoelectric sensors have demonstrated continuous real-time measurements of subtle physiological signals. Further, the development of ML technology further facilitated the practical use of the piezoelectric sensors for early detection and prevention of CVDs.[154] By providing the user with his or her health status, the user can proactively take measures to diagnose one's health condition. Even so, there are many challenges to be overcome in both aspects of the piezoelectric sensors and ML technologies.

Regarding piezoelectric sensors, first, one of the critical challenges faced by piezoelectric sensors in body pulse detection is maintaining reliable signal recording under dynamic conditions. Wearable/patchable piezoelectric sensors are required to closely contact the skin for accurate detection of the subtle vibration of body pulses. During motion, long-term use, or extreme conditions, however, the mechanical interaction between the sensor and the skin becomes complex, leading to mismatching and detachment. Furthermore, the mismatch in Young's modulus of the sensor material and the skin hampers compliant contact, resulting in signal deterioration and inaccuracies. To address this issue, researchers have proposed self-adherent ultrathin sensors that rely on van der Waals' force or chemical adherence for better contact with the skin.[155,156] However, the long-term robustness of such adherence, especially in extreme conditions like underwater activities, remains a challenge. Striking a balance between sensor adherence and skin irritation is other considerations to be made. The development of future piezoelectric sensors that can reliably monitor cardiovascular vital signs during motion, long-term usage, or under extreme conditions is eagerly anticipated to enhance wearable health monitoring technologies.[157]

Second, the incorporation of wireless data communication in wearable piezoelectric sensors has significantly improved real-time monitoring and portability, enabling continuous data collection beyond clinical or fixed locations. However, communication module such as 1–5 mW of power for Bluetooth requires power that exceeds the capabilities of small-scale batteries, which poses a significant challenge for the realization of continuous real-time health monitoring using the piezoelectric sensors. Furthermore, the utilization of inflexible commercial integrated circuit (IC) chips for signal acquisition, processing modules, and wireless data transmission often results in less adaptable systems. To tackle these challenges, intensive study needs to be done to build more conformable systems to the flexible/wearable piezoelectric sensors for efficient signal acquisition, processing, data transmission, and power supply.

Third, there are still limitations in practical use of the piezoelectric sensors for the medical diagnosis. Although the wearable piezoelectric biosensors have shown promise in monitoring cardiovascular physiological signals, their diagnostic abilities based on big data and deep learning are still in early stages. Many existing sensors may only present ECG signals or heart rate parameters without professional medical interpretation, limiting their usefulness for both users and clinicians. To achieve more comprehensive and precise medical diagnosis related to heart-related diseases, it is crucial to extract more profound parameters such as heart rate variability and cardiac output. These parameters can provide a comprehensive medical assessment with higher precision. Future piezoelectric sensors should be equipped with integrated AI algorithms to enable precise and comprehensive diagnosis, allowing users and medical professionals to make informed decisions based on comprehensive data analysis.

Regarding ML technique, in spite of huge progress in ML technology to assist data processing and diagnosing CVDs, ML-assisted processing also inherits the limitations inherent to ML algorithms. It is required to gather substantial quantities of

diverse and meticulously validated training data acquired by the sensors which otherwise deteriorate prediction accuracy of the ML model. As the quality of data directly affects the outcome of the ML algorithms fluctuations in device performances and poor long-term stability of the sensors pose a great challenge to ML technology.[158] Consequently, more sophisticated ML algorithms must be devised to streamline the training procedure, and also the sensors need to be improved to attain repeatable and uniform data. In addition, development of an appropriate ML model that aligns with the characteristics of data acquired and the intended outcomes takes precedence. Each of various ML algorithms formulated exhibits its strengths and at the same time drawbacks, which must be weighed when addressing different medical cases. Lastly, the learning process and decision-making within ML for the diagnosis of CVDs necessitate adherence to relevant knowledge and reasoning principles to ensure efficacious results for a given application.

7. Conclusion

Unlike conventional medical devices for diagnosing CVDs, flexible/wearable piezoelectric sensors have been emerged as a new generation medical sensor for the continuous and real-time health monitoring by offering portability, comfortability, and wearability. In this review, we presented the recent advances in flexible/wearable piezoelectric passive sensors for continuous and real-time heart rate and blood pressure monitoring techniques covering not only the device aspects, but also circuit design of the sensing system and ML techniques for effectively obtaining and processing reliable body pulse signals and ultimately diagnosing the CVDs. While there have been significant advances towards the realization of continuous and real-time health monitoring for CVD diagnosis, there remain challenges to be resolved: (1) attaining reliable physiological signals by the piezoelectric biosensor under dynamic, long-term use, and extreme conditions; (2) building conformable systems to the flexible/wearable piezoelectric sensors for data transmission and processing, and power supply; (3) enabling the sensors to attain more profound parameters such as heart rate variability and cardiac output; and (4) further advancing ML algorithms to streamline the training procedure and align with the characteristics of data acquired. With these improvements, it is anticipated that continuous and real-time health monitoring using the piezoelectric biosensors can be implemented in various medical practices to diagnose CVDs. We hope that this review provides insightful information in the relevant fields to the readers for the further advancements and innovations for continuous and real-time health monitoring technologies.

Author contributions

S. H., Y. G., and Y. H. contributed to conceptualization, investigation, and writing original draft preparation. F. S. and Z. J. wrote an original draft of materials' part. Y. C. contributed to conceptualization, funding acquisition, project administration, supervision, and writing.

Conflicts of interest

There are no conflicts to declare.

Acknowledgements

Y. C. thank National Natural Science Foundation of China (NSFC) for the financial support of this work (Grant number 52050410331).

Notes and references

1 J. A. Thiyagarajan, C. Mikton, R. H. Harwood, M. Gichu, V. Gaigbe-Togbe, T. Jhamba, D. Pokorna, V. Stoevska, R. Hada, G. S. Steffan, A. Liena, E. Rocard and T. Diaz, *Age Ageing*, 2022, **51**, afac147.
2 J. L. Rodgers, J. Jones, S. I. Bolleddu, S. Vanthenapalli, L. E. Rodgers, K. Shah, K. Karia and S. K. Panguluri, *J. Cardiovasc. Dev. Dis.*, 2019, **6**, 19.
3 M. Zhou, G. Zhao, Y. Zeng, J. Zhu, F. Cheng and W. Liang, *Rev. Cardiovasc. Med.*, 2022, **23**, 135.
4 S. Chen, J. Qi, S. Fan, Z. Qiao, J. C. Yeo and C. T. Lim, *Adv. Healthcare Mater.*, 2021, **10**, 2100116.
5 T. Yokota, P. Zalar, M. Kaltenbrunner, H. Jinno, N. Matsuhisa, H. Kitanosako, Y. Tachibana, W. Yukita, M. Koizumi and T. Someya, *Sci. Adv.*, 2016, **2**, e1501856.
6 C. M. Lochner, Y. Khan, A. Pierre and A. C. Arias, *Nat. Commun.*, 2014, **5**, 5745.
7 J. Kim, G. A. Salvatore, H. Araki, A. M. Chiarelli, Z. Xie, A. Banks, X. Sheng, Y. Liu, J. W. Lee, K. I. Jang, S. Y. Heo, K. Cho, H. Luo, B. Zimmerman, J. Kim, L. Yan, X. Feng, S. Xu, M. Fabiani, G. Gratton, Y. Huang, U. Paik and J. A. Rogers, *Sci. Adv.*, 2016, **2**, e1600418.
8 C. Wang, X. Li, H. Hu, L. Zhang, Z. Huang, M. Lin, Z. Zhang, Z. Yin, B. Huang, H. Gong, S. Bhaskaran, Y. Gu, M. Makihata, Y. Guo, Y. Lei, Y. Chen, C. Wang, Y. Li, T. Zhang, Z. Chen, A. P. Pisano, L. Zhang, Q. Zhou and S. Xu, *Nat. Biomed. Eng.*, 2018, **2**, 687–695.
9 J. Yang, J. Chen, Y. Su, Q. Jing, Z. Li, F. Yi, X. Wen, Z. Wang and Z. L. Wang, *Adv. Mater.*, 2015, **27**, 1316–1326.
10 H. Ouyang, J. Tian, G. Sun, Y. Zou, Z. Liu, H. Li, L. Zhao, B. Shi, Y. Fan, Y. Fan, Z. L. Wang and Z. Li, *Adv. Mater.*, 2017, **29**, 1703456.
11 C. Pang, J. H. Koo, A. Nguyen, J. M. Caves, M. G. Kim, A. Chortos, K. Kim, P. J. Wang, J. B. H. Tok and Z. Bao, *Adv. Mater.*, 2015, **27**, 634–640.
12 C. M. Boutry, A. Nguyen, Q. O. Lawal, A. Chortos, S. Rondeau-Gagné and Z. Bao, *Adv. Mater.*, 2015, **27**, 6954–6961.
13 T. Yang, X. Jiang, Y. Zhong, X. Zhao, S. Lin, J. Li, X. Li, J. Xu, Z. Li and H. Zhu, *ACS Sens.*, 2017, **2**, 967–974.
14 N. Luo, W. Dai, C. Li, Z. Zhou, L. Lu, C. C. Y. Poon, S. C. Chen, Y. Zhang and N. Zhao, *Adv. Funct. Mater.*, 2016, **6**, 1178–1187.
15 Y. Wang, S. Gong, S. J. Wang, G. P. Simon and W. Cheng, *Mater. Horiz.*, 2016, **3**, 208–213.

16 J. Chen, H. Liu, W. Wang, N. Nabulsi, W. Zhao, J. Y. Kim, M. K. Kwon and J. H. Ryou, *Adv. Funct. Mater.*, 2019, **29**, 1903162.
17 B. Dong, Z. Zhang, Q. Shi, J. Wei, Y. Ma, Z. Xiao and C. Lee, *Sci. Adv.*, 2022, **8**, eabl9874.
18 T. Jin, S.-H. K. Park and D.-W. Fan, *RSC Adv.*, 2022, **12**, 21014–21021.
19 M. Alivon, T. V. D. Phuong, V. Vignon, E. Bozec, H. Khettab, O. Hanon, M. Briet, J. M. Halimi, M. Hallab, M. Plichart, K. Mohammedi, M. Marre, P. Boutouyrie and S. Laurent, *Arch. Cardiovasc. Dis.*, 2015, **108**, 227–234.
20 Y. Hu and Z. L. Wang, *Nano Energy*, 2015, **14**, 3–14.
21 J. Wang, C. Wu, Y. Dai, Z. Zhao, A. Wang, T. Zhang and Z. L. Wang, *Nat. Commun.*, 2017, **8**, 88.
22 C. Krittanawong, A. J. Rogers, K. W. Johnson, Z. Wang, M. P. Turakhia, J. L. Halperin and S. M. Narayan, *Nat. Rev. Cardiol.*, 2021, **18**, 75–91.
23 K. H. Lee, X. Ni, J. Y. Lee, H. Arafa, D. J. Pe, S. Xu, R. Avila, M. Irie, J. H. Lee, R. L. Easterlin, D. H. Kim, H. U. Chung, O. O. Olabisi, S. Getaneh, E. Chung, M. Hill, J. Bell, H. Jang, C. Liu, J. Bin Park, J. Kim, S. B. Kim, S. Mehta, M. Pharr, A. Tzavelis, J. T. Reeder, I. Huang, Y. Deng, Z. Xie, C. R. Davies, Y. Huang and J. A. Rogers, *Nat. Biomed. Eng.*, 2020, **4**, 148–158.
24 J. Hu, G. Dun, X. Geng, J. Chen, X. Wu and T.-L. Ren, *Nanoscale Adv.*, 2023, **5**, 3131–3145.
25 R. Lay, G. S. Deijs and J. Malmström, *RSC Adv.*, 2021, **11**, 30657–30673.
26 S. Panda, S. Hajra, K. Mistewicz, P. In-na, M. Sahu, P. M. Rajaitha and H. J. Kim, *Nano Energy*, 2022, **100**, 107514.
27 C. R. Bowen, H. A. Kim, P. M. Weaver and S. Dunn, *Energy Environ. Sci.*, 2014, **7**, 25–44.
28 S. Mohammadpourfazeli, S. Arash, A. Ansari, S. Yang, K. Mallick and R. Bagherzadeh, *RSC Adv.*, 2023, **13**, 370–387.
29 S. Trolier-Mckinstry, S. Zhang, A. J. Bell and X. Tan, *Annu. Rev. Mater. Res.*, 2018, **48**, 191–217.
30 H. Liu, J. Zhong, C. Lee, S. W. Lee and L. Lin, *Appl. Phys. Rev.*, 2018, **5**, 041306.
31 N. Sezer and M. Koç, *Nano Energy*, 2021, **80**, 105567.
32 M. T. Chorsi, E. J. Curry, H. T. Chorsi, R. Das, J. Baroody, P. K. Purohit, H. Ilies and T. D. Nguyen, *Adv. Mater.*, 2019, **31**, 1802084.
33 D. Damjanovic, *Appl. Phys. Lett.*, 2010, **97**, 062906.
34 D. Damjanovic, *J. Am. Ceram. Soc.*, 2005, **88**, 2663–2676.
35 C. A. Randall, G. A. Rossetti and W. Cao, *Ferroelectr*, 1993, **150**, 163–169.
36 G. A. Rossetti, L. E. Cross and J. P. Cline, *J. Mater. Sci.*, 1995, **30**, 24–34.
37 D. A. Hall, *J. Mater. Sci.*, 2001, **36**, 4575–4601.
38 X. L. Zhang, Z. X. Chen, L. E. Cross and W. A. Schulze, *J. Mater. Sci.*, 1983, **18**, 968–972.
39 S. Trolier-McKinstry, N. Bassiri Gharb and D. Damjanovic, *Appl. Phys. Lett.*, 2006, **88**, 202901.
40 N. Bassiri-Gharb, S. Trolier-Mckinstry and D. Damjanovic, *J. Appl. Phys.*, 2011, **110**, 124104.
41 C. A. Randall, N. Kim, J. P. Kucera, W. Cao and T. R. Shrout, *J. Am. Ceram. Soc.*, 1998, **81**, 677–688.
42 D. M. Marincel, H. Zhang, S. Jesse, A. Belianinov, M. B. Okatan, S. V. Kalinin, W. M. Rainforth, I. M. Reaney, C. A. Randall and S. Trolier-Mckinstry, *J. Am. Ceram. Soc.*, 2015, **98**, 1848–1857.
43 R. Lay, G. S. Deijs and J. Malmström, *RSC Adv.*, 2021, **11**, 30657–30673.
44 Y. Terai, K. Haraguchi, R. Ichinose, H. Oota and K. Yonezawa, *Jpn. J. Appl. Phys.*, 2022, **62**, SA1003.
45 I. L. Guy, S. Muensit and E. M. Goldys, *Appl. Phys. Lett.*, 1999, **75**, 4133–4135.
46 A. F. L. Almeida, P. B. A. Fechine, J. C. Góes, M. A. Valente, M. A. R. Miranda and A. S. B. Sombra, *Mater. Sci. Eng. B Solid State Mater. Adv. Technol.*, 2004, **111**, 113–123.
47 J. Hao, W. Li, J. Zhai and H. Chen, *Mater. Sci. Eng., R*, 2019, **135**, 1–57.
48 T. Karaki, K. Yan, T. Miyamoto and M. Adachi, *Jpn. J. Appl. Phys.*, 2007, **46**, L97.
49 K. S. Ramadan, D. Sameoto and S. Evoy, *Smart Mater. Struct.*, 2014, **23**, 033001.
50 M. Huang, M. Zhu, X. Feng, Z. Zhang, T. Tang, X. Guo, T. Chen, H. Liu, L. Sun and C. Lee, *ACS Nano*, 2023, **17**, 6435–6451.
51 D. J. Shin, S. J. Jeong, C. E. Seo, K. H. Cho and J. H. Koh, *Ceram. Int.*, 2015, **41**, S686–S690.
52 K. Kapat, Q. T. H. Shubhra, M. Zhou and S. Leeuwenburgh, *Adv. Funct. Mater.*, 2020, **30**, 1909045.
53 Y. Guo, K. I. Kakimoto and H. Ohsato, *Mater. Lett.*, 2005, **59**, 241–244.
54 S. T. Zhang, A. B. Kounga, E. Aulbach, T. Granzow, W. Jo, H. J. Kleebe and J. Rödel, *J. Appl. Phys.*, 2008, **103**, 034108.
55 R. Wang, R. J. Xie, K. Hanada, K. Matsusaki, H. Kawanaka, H. Bando, T. Sekiya and M. Itoh, *J. Electroceram.*, 2008, **21**, 263–266.
56 Jamal Kazmi, P. C. Ooi, B. T. Goh, M. K. Lee, M. F. M. R. Wee, S. S. A Karim, S. R. A. Raza and M. A. Mohamed, *RSC Adv.*, 2020, **10**, 23297–23311.
57 K. Davis, R. Yarbrough, M. Froeschle, J. White and H. Rathnayake, *RSC Adv.*, 2019, **9**, 14638–14648.
58 R. E. Newnham, *Properties of Materials: Anisotropy, Symmetry, Structure*, Oxford University Press, New York, NY, USA, 2005.
59 R. Kumar, O. Al-Dossary, G. Kumar and A. Umar, *Nanomicro Lett.*, 2015, **7**, 97–120.
60 Y. Cho, J. B. Park, B. S. Kim, J. Lee, W. K. Hong, I. K. Park, J. E. Jang, J. I. Sohn, S. N. Cha and J. M. Kim, *Nano Energy*, 2015, **16**, 524–532.
61 Y. Cho, D. Ahn, J. B. Park, S. Pak, S. Lee, B. O. Jun, J. Hong, S. Y. Lee, J. E. Jang, J. Hong, S. M. Morris, J. I. Sohn, S. N. Cha and J. M. Kim, *Adv. Electron. Mater.*, 2016, **2**, 1600225.
62 Y. Cho, S. Pak, Y. G. Lee, J. S. Hwang, P. Giraud, G. H. An and S. N. Cha, *Adv. Funct. Mater.*, 2020, **30**, 1908479.
63 Y. Cho, S. Pak, B. Li, B. Hou and S. N. Cha, *Adv. Funct. Mater.*, 2021, **31**, 2104239.

64 Y. Cho, B. Hou, P. Giraud, S. Pak and S. Cha, *ACS Appl. Energy Mater.*, 2021, **4**, 12056–12062.
65 Y. Cho, S. Lee, J. Hong, S. Pak, B. Hou, Y. W. Lee, J. E. Jang, H. Im, J. I. Sohn, S. Cha and J. M. Kim, *J. Mater. Chem. A*, 2018, **6**, 12440–12446.
66 Y. Cho, P. Giraud, B. Hou, Y. W. Lee, J. Hong, S. Lee, S. Pak, J. Lee, J. E. Jang, S. M. Morris, J. I. Sohn, S. N. Cha and J. M. Kim, *Adv. Energy Mater.*, 2018, **8**, 1700809.
67 J. Lee, F. Shen, S. Miao, G. H. Ryu, B. Im, D. G. Kim, G. H. An and Y. Cho, *Nano Energy*, 2022, **104**, 107891.
68 H. Kawai, *Jpn. J. Appl. Phys.*, 1969, **8**, 975.
69 S. Sukumaran, S. Chatbouri, D. Rouxel, E. Tisserand, F. Thiebaud and T. Ben Zineb, *J. Intell. Mater. Syst. Struct.*, 2021, **32**, 746–780.
70 Y. Xin, H. Sun, H. Tian, C. Guo, X. Li, S. Wang and C. Wang, *Ferroelectrics*, 2016, **502**, 28–42.
71 L. Seminara, M. Capurro, P. Cirillo, G. Cannata and M. Valle, *Sens. Actuators, A*, 2011, **169**, 49–58.
72 N. A. Shepelin, A. M. Glushenkov, V. C. Lussini, P. J. Fox, G. W. Dicinoski, J. G. Shapter and A. V. Ellis, *Energy Environ. Sci.*, 2019, **12**, 1143–1176.
73 A. J. Lovinger, D. D. Davis, R. E. Cais and J. M. Kometani, *Polymer*, 1987, **28**, 617–626.
74 T. Furukawa, M. Date, E. Fukada, Y. Tajitsu and A. Chiba, *Jpn. J. Appl. Phys.*, 1980, **19**, L109.
75 T. Yamada, T. Ueda and T. Kitayama, *J. Appl. Phys.*, 1981, **52**, 948–952.
76 Y. Higashihata, J. Sako and T. Yagi, *Ferroelectrics*, 1981, **32**, 61–67.
77 N. A. Shepelin, A. M. Glushenkov, V. C. Lussini, P. J. Fox, G. W. Dicinoski, J. G. Shapter and A. V. Ellis, *Energy Environ. Sci.*, 2019, **12**, 1143–1176.
78 A. Sultana, S. K. Ghosh, V. Sencadas, T. Zheng, M. J. Higgins, T. R. Middya and D. Mandal, *J. Mater. Chem. B*, 2017, **5**, 7352–7359.
79 T. Yoshida, K. Imoto, T. Nakai, R. Uwami, T. Kataoka, M. Inoue, T. Fukumoto, Y. Kamimura, A. Kato and Y. Tajitsu, *Jpn. J. Appl. Phys.*, 2011, **50**, 09ND13.
80 M. Tsukiji, H. Kowa and K. Muraki, *Jpn. J. Appl. Phys.*, 1998, **37**, 3374.
81 T. Yucel, P. Cebe and D. L. Kaplan, *Adv. Funct. Mater.*, 2011, **21**, 779–785.
82 D. M. Shin, S. W. Hong and Y. H. Hwang, *Nanomaterials*, 2020, **10**, 123.
83 S. J. Heerema and C. Dekker, *Nat. Nanotechnol.*, 2016, **11**, 127–136.
84 S. Xu, J. Zhan, B. Man, S. Jiang, W. Yue, S. Gao, C. Guo, H. Liu, Z. Li, J. Wang and Y. Zhou, *Nat. Commun.*, 2017, **8**, 14902.
85 G. Da Cunha Rodrigues, P. Zelenovskiy, K. Romanyuk, S. Luchkin, Y. Kopelevich and A. Kholkin, *Nat. Commun.*, 2015, **6**, 7572.
86 T. Li and P. S. Lee, *Small Struct.*, 2022, **3**, 2100128.
87 Y. Takano, R. Hayakawa, M. Suzuki and S. Kakio, *Jpn. J. Appl. Phys.*, 2021, **60**, SDDC08.
88 Z. Yang and J. Zu, *Energy Convers. Manage.*, 2016, **122**, 321–329.
89 D. Biswas, P. Sharma and N. S. Panwar, *Ferroelectr*, 2020, **571**, 214–229.
90 P. H. Townsend, S. J. Martin, J. Godschalx, D. R. Romer, D. W. Smith Jr., D. Castillo, R. DeVries, G. Buske, N. Rondan, S. Froelicher, J. Marshall, E. O. Shaffer and J.-H. Im, *Mater. Res. Soc. Symp. Proc.*, 1997, **9**, 476.
91 X. Wang, L. Dong, H. Zhang, R. Yu, C. Pan and Z. L. Wang, *Adv. Sci.*, 2015, **2**, 1500169.
92 Y. Zang, F. Zhang, C. A. Di and D. Zhu, *Mater. Horiz.*, 2015, **2**, 140–156.
93 M. Amjadi, K. U. Kyung, I. Park and M. Sitti, *Adv. Funct. Mater.*, 2016, **26**, 1678–1698.
94 H. Souri, H. Banerjee, A. Jusufi, N. Radacsi, A. A. Stokes, I. Park, M. Sitti and M. Amjadi, *Adv. Intell. Syst.*, 2020, **2**, 2000039.
95 L. Pan, A. Chortos, G. Yu, Y. Wang, S. Isaacson, R. Allen, Y. Shi, R. Dauskardt and Z. Bao, *Nat. Commun.*, 2014, **5**, 3002.
96 M. L. Hammock, A. Chortos, B. C. K. Tee, J. B. H. Tok and Z. Bao, *Adv. Mater.*, 2013, **25**, 5997–6038.
97 S. Xu, Y. Qin, C. Xu, Y. Wei, R. Yang and Z. L. Wang, *Nat. Nanotechnol.*, 2010, **5**, 366–373.
98 L. Lin, Y. Xie, S. Wang, W. Wu, S. Niu, X. Wen and Z. L. Wang, *ACS Nano*, 2013, **7**, 8266–8274.
99 F. R. Fan, Z. Q. Tian and Z. Lin Wang, *Nano Energy*, 2012, **1**, 328–334.
100 S. Wang, L. Lin and Z. L. Wang, *Nano Lett.*, 2012, **12**, 6339–6346.
101 Y. Wang, Y. Yu, X. Wei and F. Narita, *Adv. Mater. Technol.*, 2022, **7**, 2200318.
102 Z. Alizadeh Sani, A. Shalbaf, H. Behnam and R. Shalbaf, *J. Digit. Imaging*, 2015, **28**, 91–98.
103 J. J. Shu and Y. Sun, *Med. Complement. Ther.*, 2007, **15**, 190–198.
104 K. Meng, X. Xiao, W. Wei, G. Chen, A. Nashalian, S. Shen, X. Xiao and J. Chen, *Adv. Mater.*, 2022, **34**, 2109357.
105 Z. Yi, Z. Liu, W. Li, T. Ruan, X. Chen, J. Liu, B. Yang and W. Zhang, *Adv. Mater.*, 2022, **34**, 2110291.
106 Y. Fang, Y. Zou, J. Xu, G. Chen, Y. Zhou, W. Deng, X. Zhao, M. Roustaei, T. K. Hsiai and J. Chen, *Adv. Mater.*, 2021, **33**, 2104178.
107 J. Hou, Y. Zhang, S. Zhang, X. Geng, J. Zhang, C. Chen and H. Zhang, *Comput. Methods Programs Biomed.*, 2020, **189**, 105321.
108 G. D'ambrogio, O. Zahhaf, M. Bordet, M. Q. Le, N. D. Schiava, R. Liang, P.-J. Cottinet and J.-F. Capsal, *Adv. Eng. Mater.*, 2021, **23**, 2100341.
109 S. Chen, N. Wu, S. Lin, J. Duan, Z. Xu, Y. Pan, H. Zhang, Z. Xu, L. Huang, B. Hu and J. Zhou, *Nano Energy*, 2020, **70**, 104460.
110 K. Meng, J. Chen, X. Li, Y. Wu, W. Fan, Z. Zhou, Q. He, X. Wang, X. Fan, Y. Zhang, J. Yang and Z. L. Wang, *Adv. Funct. Mater.*, 2019, **29**, 1806388.
111 G. Chen, C. Au and J. Chen, *Trends Biotechnol.*, 2021, **39**, 1078–1092.
112 B. Trachet, P. Reymond, J. Kips, A. Swillens, M. De Buyzere, B. Suys, N. Stergiopulos and P. Segers, *Ann. Biomed.*, 2010, **38**, 876–888.

113 S. A. M. Huybrechts, D. G. Devos, S. J. Vermeersch, D. Mahieu, E. Achten, T. L. M. De Backer, P. Segers and L. M. Van Bortel, *J. Hypertens.*, 2011, **29**, 1577–1582.
114 J.-H. Li, J. hui Chen and F. Xu, *Adv. Mater. Technol.*, 2018, **3**, 1800296.
115 S. C. Millasseau, R. P. Kelly, J. M. Ritter and P. J. Chowienczyk, *Clin. Sci.*, 2002, **103**, 371–377.
116 T. Yang, X. Jiang, Y. Zhong, X. Zhao, S. Lin, J. Li, X. Li, J. Xu, Z. Li and H. Zhu, *ACS Sens.*, 2017, **2**, 967–974.
117 M. Brennan, M. Palaniswami and P. Kamen, *IEEE Trans. Biomed. Eng.*, 2001, **48**, 1342–1347.
118 D. Y. Park, D. J. Joe, D. H. Kim, H. Park, J. H. Han, C. K. Jeong, H. Park, J. G. Park, B. Joung and K. J. Lee, *Adv. Mater.*, 2017, **29**, 1702308.
119 R. Fu, L. Tu, Y. Zhou, L. Fan, F. Zhang, Z. Wang, J. Xing, D. Chen, C. Deng, G. Tan, P. Yu, L. Zhou and C. Ning, *Chem. Mater.*, 2019, **31**, 9850–9860.
120 R. Sun, S. C. Carreira, Y. Chen, C. Xiang, L. Xu, B. Zhang, M. Chen, I. Farrow, F. Scarpa and J. Rossiter, *Adv. Mater. Technol.*, 2019, **4**, 1900100.
121 P. Samartkit, S. Pullteap and O. Bernal, *Measurement*, 2022, **196**, 111211.
122 S. Wu, P. Dong, X. Cui and Y. Zhang, *Nano Energy*, 2022, **96**, 107136.
123 L. Yu, J. C. Yeo, R. H. Soon, T. Yeo, H. H. Lee and C. T. Lim, *ACS Appl. Mater. Interfaces*, 2018, **10**, 12773–12780.
124 L. Yu, Y. Feng, L. Yao, R. H. Soon, J. C. Yeo and C. T. Lim, *ACS Appl. Mater. Interfaces*, 2019, **11**, 33347–33355.
125 Z. Yi, W. Zhang and B. Yang, *J. Manuf. Syst.*, 2022, **32**, 103003.
126 G.-T. Hwang, H. Park, J.-H. Lee, S. Oh, K.-I. Park, M. Byun, H. Park, G. Ahn, C. K. Jeong, K. No, H. Kwon, S.-G. Lee, B. Joung and K. J. Lee, *Adv. Mater.*, 2014, **26**, 4880–4887.
127 X. Cheng, B. Meng, X. Zhang, M. Han, Z. Su and H. Zhang, *Nano Energy*, 2015, **12**, 19–25.
128 W. Tang, J. Tian, Q. Zheng, L. Yan, J. Wang, Z. Li and Z. L. Wang, *ACS Nano*, 2015, **9**, 7867–7873.
129 X. Cheng, X. Xue, Y. Ma, M. Han, W. Zhang, Z. Xu, H. Zhang and H. Zhang, *Nano Energy*, 2016, **22**, 453–460.
130 P. Tan, Y. Xi, S. Chao, D. Jiang, Z. Liu, Y. Fan and Z. Li, *Biosensors*, 2022, **12**, 234.
131 Z. D. Liu, J. K. Liu, B. Wen, Q. Y. He, Y. Li and F. Miao, *Sensors*, 2018, **18**, 4227.
132 M. Kachuee, M. M. Kiani, H. Mohammadzade and M. Shabany, *IEEE Trans. Biomed. Eng.*, 2017, **64**, 859–869.
133 H. Li, Y. Ma, Z. Liang, Z. Wang, Y. Cao, Y. Xu, H. Zhou, B. Lu, Y. Chen, Z. Han, S. Cai and X. Feng, *Natl. Sci. Rev.*, 2020, **7**, 849–862.
134 K. Maity, S. Garain, K. Henkel, D. Schmeißer and D. Mandal, *ACS Appl. Polym. Mater.*, 2020, **2**, 862–878.
135 S. Min, D. H. Kim, D. J. Joe, B. W. Kim, Y. H. Jung, J. H. Lee, B. Y. Lee, I. Doh, J. An, Y. N. Youn, B. Joung, C. D. Yoo, H. S. Ahn and K. J. Lee, *Adv. Mater.*, 2023, **35**, 2301627.
136 T. W. Wang and S. F. Lin, *Sensors*, 2020, **20**, 851.
137 W. B. White, A. S. Berson, C. Robbins, M. J. Jamieson, L. M. Prisant, E. Roccella and S. G. Sheps, *Hypertension*, 1993, **21**, 504–509.
138 E. O'brien, J. Petrie, W. Littler, M. De Swiet, P. L. Padfield, D. G. Altmanu, M. Blandg, A. Coats and N. Atkins, *J. Hypertens.*, 1993, **11**, S43–S62.
139 A. Miller and P. D. White, *Am. Heart J.*, 1941, **21**, 22–26.
140 Z. Yi, J. Huang, Z. Liu, J. Liu and B. Yang, *IEEE Electron Device Lett.*, 2020, **41**, 183–186.
141 Z. Yi, H. Yang, Y. Tian, X. Dong, J. Liu and B. Yang, *IEEE Electron Device Lett.*, 2018, **39**, 1226–1229.
142 F. Ershad, A. Thukral, J. Yue, P. Comeaux, Y. Lu, H. Shim, K. Sim, N. I. Kim, Z. Rao, R. Guevara, L. Contreras, F. Pan, Y. Zhang, Y. S. Guan, P. Yang, X. Wang, P. Wang, X. Wu and C. Yu, *Nat. Commun.*, 2020, **11**, 3823.
143 C. Wang, X. Li, H. Hu, L. Zhang, Z. Huang, M. Lin, Z. Zhang, Z. Yin, B. Huang, H. Gong, S. Bhaskaran, Y. Gu, M. Makihata, Y. Guo, Y. Lei, Y. Chen, C. Wang, Y. Li, T. Zhang, Z. Chen, A. P. Pisano, L. Zhang, Q. Zhou and S. Xu, *Nat. Biomed. Eng.*, 2018, **2**, 687–695.
144 X. Xi and D. D. L. Chung, *Carbon*, 2019, **150**, 531–548.
145 M. M. A. C. Moreira, I. N. Soares, Y. A. O. Assagra, F. S. I. Sousa, T. M. Nordi, D. M. Dourado, R. H. Gounella, J. P. Carmo, R. A. C. Altafim and R. A. P. Altafim, *IEEE Sens. J.*, 2021, **21**, 22317–22328.
146 Y. Chu, J. Zhong, H. Liu, Y. Ma, N. Liu, Y. Song, J. Liang, Z. Shao, Y. Sun, Y. Dong, X. Wang and L. Lin, *Adv. Funct. Mater.*, 2018, **28**, 1803413.
147 Y. Wang, M. L. Adam, Y. Zhao, W. Zheng, L. Gao, Z. Yin and H. Zhao, *Nanomicro Lett.*, 2023, **15**, 55.
148 S. H. Kwon and L. Dong, *Nano Energy*, 2022, **102**, 107632.
149 Y. Himeur, A. Alsalemi, F. Bensaali, A. Amira and A. Al-Kababji, *Int. J. Intell. Syst.*, 2022, **37**, 7124–7179.
150 L. Alzubaidi, J. Zhang, A. J. Humaidi, A. Al-Dujaili, Y. Duan, O. Al-Shamma, J. Santamaría, M. A. Fadhel, M. Al-Amidie and L. Farhan, *J. Big Data*, 2021, **8**, 1–74.
151 Y. H. Jung, S. K. Hong, H. S. Wang, J. H. Han, T. X. Pham, H. Park, J. Kim, S. Kang, C. D. Yoo and K. J. Lee, *Adv. Mater.*, 2020, **32**, 1904020.
152 M. Belgiu and L. Drăgu, *ISPRS J. Photogramm. Remote Sens.*, 2016, **114**, 24–31.
153 K. H. Huang, F. Tan, T. D. Wang and Y. J. Yang, *Sensors*, 2019, **19**, 848.
154 S. Chen, J. Qi, S. Fan, Z. Qiao, J. C. Yeo and C. T. Lim, *Adv. Healthcare Mater.*, 2021, **10**, 2100116.
155 T. Ha, J. Tran, S. Liu, H. Jang, H. Jeong, R. Mitbander, H. Huh, Y. Qiu, J. Duong, R. L. Wang, P. Wang, A. Tandon, J. Sirohi and N. Lu, *Adv. Sci.*, 2019, **6**, 1900290.
156 C. Zhang, J. Chen, W. Xuan, S. Huang, B. You, W. Li, L. Sun, H. Jin, X. Wang, S. Dong, J. Luo, A. J. Flewitt and Z. L. Wang, *Nat. Commun.*, 2020, **11**, 58.
157 S. Ji, C. Wan, T. Wang, Q. Li, G. Chen, J. Wang, Z. Liu, H. Yang, X. Liu and X. Chen, *Adv. Mater.*, 2020, **32**, 2001496.
158 T. Kim, Y. Shin, K. Kang, K. Kim, G. Kim, Y. Byeon, H. Kim, Y. Gao, J. R. Lee, G. Son, T. Kim, Y. Jun, J. Kim, J. Lee, S. Um, Y. Kwon, B. G. Son, M. Cho, M. Sang, J. Shin, K. Kim, J. Suh, H. Choi, S. Hong, H. Cheng, H.-G. Kang, D. Hwang and K. J. Yu, *Nat. Commun.*, 2022, **13**, 5815.